



저작자표시-비영리-변경금지 2.0 대한민국

이용자는 아래의 조건을 따르는 경우에 한하여 자유롭게

- 이 저작물을 복제, 배포, 전송, 전시, 공연 및 방송할 수 있습니다.

다음과 같은 조건을 따라야 합니다:



저작자표시. 귀하는 원저작자를 표시하여야 합니다.



비영리. 귀하는 이 저작물을 영리 목적으로 이용할 수 없습니다.



변경금지. 귀하는 이 저작물을 개작, 변형 또는 가공할 수 없습니다.

- 귀하는, 이 저작물의 재이용이나 배포의 경우, 이 저작물에 적용된 이용허락조건을 명확하게 나타내어야 합니다.
- 저작권자로부터 별도의 허가를 받으면 이러한 조건들은 적용되지 않습니다.

저작권법에 따른 이용자의 권리는 위의 내용에 의하여 영향을 받지 않습니다.

이것은 [이용허락규약\(Legal Code\)](#)을 이해하기 쉽게 요약한 것입니다.

[Disclaimer](#)

Synthesis and cell-imaging applications of water-soluble BODIPY dyes

Supervisor Prof. Kim Ho-Joong

This thesis is submitted in partial fulfillment
of the requirements for the
Master of Science in Chemistry.

April 2019

Chosun University Graduate School

Department of Chemistry

Badon, Isabel Wen T.

Confirmation of Master' s Thesis

위원장 조선대학교 교수 이 종 대 (인)

위 원 조선대학교 교수 임 종 국 (인)

위 원 조선대학교 교수 김 호 중 (인)

May 2019

Chosun University Graduate
School

Table of Contents

Table of Contents	i
LIST OF PUBLICATIONS	iv
LIST OF TABLES	v
LIST OF PICTURES	vi
LIST OF FIGURES	vii
ABSTRACT	ix
1. Introduction	1
1.1. Basic Principles of Fluorescence	1
1.2. Stokes shift	2
1.3. Inner Filter Effect	3
1.4. Fluorescence Lifetime	3
1.5. Fluorescence Quantum Yield	4
1.6. Fluorophore Structure and Property	5
2. BODIPY dyes	6
2.1. Synthesis and General Features	6
2.2. BODIPY dyes for bioimaging	9
2.3. Near-Infrared BODIPY dyes	11
2.4. Other BODIPY dyes with enhanced photophysical properties	12

CHAPTER 2: Synthesis and Photophysical Characterization of Highly Water-Soluble PEGylated BODIPY Derivatives for Cellular Imaging

1	Introduction	14
2	Experimental	15
2.1	Synthesis of halogenated dyes	16
2.2	Synthesis of poly(ethylene glycol) methyl ether tosylate	17
2.3	Synthesis of ethyl-3,5-dialkoxy benzoate	17
2.4	Synthesis of 3,5-dialkoxy benzoic acid	17
2.5	Synthesis of PEGylated BODIPY dyes	18
2.6	Cell proliferation assay	18
2.7	Confocal microscopy	19
3	Results and Discussion	19
3.1	Synthesis	19
3.2	Photophysical Properties	20
3.3	Cell viability and Imaging	24
4	Conclusion	25
<h2 style="text-align: center;">CHAPTER 3: Multi-Responsive Hydrogels Functionalized with a Photochromic Spiropyran-Conjugated Chitosan Network</h2>		
1	Introduction	35
2	Experimental	36
2.1	Synthesis of SP-functionalized IPN Hydrogel	37

2.2 Isomerization of spiropyran when exposed to light and gases	37
3 Results and Discussion	38
4 Conclusion	41
References	43
Acknowledgments	49

LIST OF PUBLICATIONS

Badon, Isabel Wen, Joomin Lee, Temmy Pagarro Vales, Byoung Ki Cho, and Ho-Joong Kim. "Synthesis and photophysical characterization of highly water-soluble PEGylated BODIPY derivatives for cellular imaging." *Journal of Photochemistry and Photobiology A: Chemistry* 377 (2019): 214-219.

Vales, Temmy Pagarro, Isabel Wen T. Badon, and Ho-Joong Kim. "Multi-Responsive Hydrogels Functionalized with a Photochromic Spiropyran-Conjugated Chitosan Network." *Macromolecular Research* 26, no. 10 (2018): 950-953.

Lee, Cheol Woo, Isabel Wen Badon, Boram Kim, Geun-Chang Ryu, and Ho-Joong Kim. "Fabrication of Spiropyran-functionalized Photochromic Hydrogel Lenses." *조선자연과학논문집* 11, no. 1 (2018): 39-43.

LIST OF TABLES

- Table 1 Photophysical properties of BOD-PEG and EtBOD-PEG dyes
- Table 2 Fluorescence quantum yields of BOD-PEG and EtBOD-PEG dyes

LIST OF PICTURES

- Picture 1 Photograph of BOD-PEG and EtBOD-PEG under UV light
- Picture 2 CLSM images of MCF-7 cells with BOD-PEG and EtBOD-PEG
- Picture 3 Visual changes in SP-IPN-H upon light irradiation
- Picture 4 Visual changes in SP-IPN-H in response to light irradiation and acid/base gas treatment

LIST OF FIGURES

- Figure 1 Jablonski energy diagram
- Figure 2 Instrumental setup for a fluorescence spectrometer and of an integrating sphere
- Figure 3 Rigid molecules and AIE molecules
- Figure 4 Scheme of synthesizing BODIPY
- Figure 5 IUPAC numbering of BODIPY structure and substitution results
- Figure 6 Structure, absorption and emission wavelength of BODIPY
- Figure 7 HOMO and LUMO of BODIPY
- Figure 8 Some examples of BODIPY dyes for cell imaging
- Figure 9 Aza-BODIPY dyes as NIR emitting dyes
- Figure 10 Di-styryl modified BODIPY as NIR emitting dyes
- Figure 11 BODIPY dyes with large Stokes shift
- Figure 12 Synthetic scheme for BOD-PEG and EtBOD-PEG
- Figure 13 Absorption and emission spectra of BOD-PEG
- Figure 14 Absorption and emission spectra of EtBOD-PEG
- Figure 15 Emission spectra of BOD-PEG and EtBOD-PEG in water
- Figure 16 Cell viability of BOD-PEG and EtBOD

LIST OF FIGURES

- Figure 17 Reversible spiropyran–merocyanine isomerization in response to light irradiation
- Figure 18 Preparation of SP–functionalized chitosan–IPN hydrogels and the structural conversion of SP with light and gases
- Figure 19 Absorbance and fluorescence spectra of SP–IPN–H before and after UV irradiation
- Figure 20 Changes in the spiropyran structure with light irradiation and exposure to acid/base gases
- Figure 21 Absorbance and fluorescence spectra of SP–IPN–H

ABSTRACT

Synthesis and cell-imaging applications of water-soluble BODIPY dyes

Badon, Isabel Wen T.

Advisor: Prof. Kim, Ho-Joong, Ph. D.

Department of Chemistry

Graduate School of Chosun University

A series of poly(ethylene glycol) (PEG)-modified water-soluble boron dipyrromethene (BODIPY) dyes (EtBODPEG and BOD-PEG) were synthesized and their photophysical properties in various solutions were investigated. The presence of ethyl groups at the 2,6-positions of the BODIPY core in EtBOD-PEG resulted in bathochromic shifts in both the absorption and emission spectra relative to those of the unsubstituted BOD-PEG. Importantly, bulky di-branched PEG chains were introduced at the meso position of the BODIPY core, leading to enhanced solubilities and high fluorescence quantum yields in aqueous solutions. The water-soluble BODIPY dyes were explored for their applicability in fluorescent bio-imaging using MCF-7 human breast cancer cells. The dyes were cell-permeable and were concentrated in cellular cytoplasm area, suggesting that they have potential applications as bio-imaging agents.

Chapter 1: Fluorescence

1. Introduction

1.1. Basic Principles of Fluorescence

When a molecule emits light of a certain wavelength upon irradiation by light of a shorter wavelength, that molecule is said to be fluorescent. Fluorescence is commonly produced by single-photon excitation, wherein a number of molecules excited by an appropriate wavelength of light absorb enough photons to promote an electron from the ground-state energy level (S_0) to an excited-state energy level (S_1).¹ When this excited electron relaxes back to the ground state energy level, it emits a photon of lower energy than the absorbed one. This transition from the excited state (S_1) to the ground state (S_0) is characterized by i) fluorescence intensity as a function of wavelength, ii) fluorescence quantum yield, and iii) fluorescence lifetime.



Where:

S_0 -ground-state energy level

S_1 -first electronically excited energy level

$h\nu$ - photon energy

The process of fluorescence is better understood using a Jablonski energy diagram as shown in Figure 1. When an electron is excited, several processes compete to de-excite it to the ground state, which are fluorescence, internal conversion or vibrational relaxation, intersystem crossing from singlet state to triplet state and phosphorescence. Each of these processes is can occur at certain probabilities associated with decay rate constants (k). Hence, the weaker the alternative pathways, the higher the relaxation *via* fluorescence. Interestingly, even if the fluorophore is excited into different singlet state energies (i.e. S_1 , S_2 , S_3 , etc.), thermal relaxation will eventually bring the fluorophore to the first electronic state (S_1) where emission can occur. This is the reason behind the independence of the emission spectrum from the excitation wavelength.²

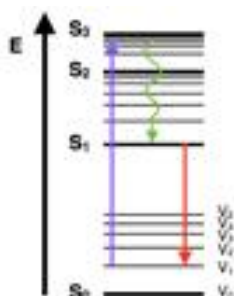


Figure 1. Jablonski energy diagram showing absorbance (purple), vibrational relaxation (green) and fluorescence (orange). Source: chem.libretexts.org

The fluorescence spectrum can be used to characterize a molecule. The intensity, position of the emission wavelength and fluorescence lifetime are some of the properties of a molecule that can be gathered through fluorescence emission. There are intrinsic properties unique for each fluorophore and can be modified by the environment.

1.2. Stokes shift

The Stokes shift, the wavelength difference between absorbance and emission peak maxima, is an important parameter for fluorescent dyes.³ This shift to longer wavelength was first observed by Sir George Stokes in 1852. Stokes shift stems from the fact that at room temperature, ground state fluorophores are generally in the lowest vibrational level of the first electronic state as explained previously. With E_a and E_{em} to describe absorption and emission energies, respectively, it can be shown that:

$$(3) \quad E_a = hc/\lambda_a$$

$$(4) \quad E_{em} = hc/\lambda_{em}$$

Due to the competitive radiative and non-radiative processes,

$$(5) \quad E_{em} < E_a$$

$$(6) \text{ Hence, } \lambda_{em} > \lambda_a$$

On some applications, a large Stokes shift is favored to minimize the overlap between the absorption and emission spectra.⁴ The lower the Stokes shift, the greater the overlap will be between the absorption and emission spectra, resulting to loss due to reabsorption of emitted

photons. Hence, to minimize reabsorption of emitted photons, Stokes shifts greater than 80 nm are desirable.⁵

1.3. Inner Filter Effect

Another consideration to make when measuring fluorescence is the effect of the optical density of the sample on the observed signal. As much as fluorescence is a popular method to studying various compounds, a crucial obstacle in using this property lies in the nonlinear dependence of fluorescence intensity to the concentration of the fluorescent compounds. This effect is called the “inner-filter effect” (IFE) and results to incorrect use of the method even by experienced researchers.⁶ The IFE is classified into the primary inner filter effect (PIFE) and the secondary inner filter effect (SIFE). The PIFE is the attenuation of the excitation beam as it reaches each subsequent layer of the solution due to the absorption of the chromophores, whereas the SIFE is the reabsorption of emitted photons by other surrounding chromophores.⁷ However, this effect can be minimized by diluting the solution or by incorporating a correction factor in the mathematical model of filter effects.⁸

1.4. Fluorescence lifetime

Fluorescence lifetime is defined as the time needed to reduce a population of excited fluorophores through fluorescence and other non-radiative processes.⁹ This time varies from nanoseconds (10^{-9} s) to (10^{-12} s) and is shown by the equation:

$$(7) \quad \tau_f = \frac{1}{k} = \frac{1}{k_r + k_{ISC} + k_I}$$

Where:

τ_f = fluorescence lifetime

The equation for fluorescence lifetime accounts for both radiative and non-radiative processes involved in the relaxation of the electron.

Fluorescence lifetime is an intrinsic property of a fluorophore and is independent on initial perturbation conditions, duration of light exposure, one- or multi-photon excitation, and photobleaching. Moreover, it is not affected by fluorescence intensity and fluorophore concentration. Since fluorescence lifetime is associated with energetically unstable states, it can be sensitive to various internal and external factors such as fluorophore structure, temperature, polarity and presence of fluorescence quenchers.⁹

1.5. Fluorescence quantum yield

After molecules in the ground state absorb energy and electrons are promoted to an excited state (S_n), different relaxation processes, including fluorescence, will compete.¹⁰ The rate constant (k) of the excited state includes the kinetic constants of the competing relaxation processes:

$$(8) \quad k = k_r + k_{ISC} + k_I$$

The fluorescence quantum yield (ϕ_F) is a measure of the number of photons emitted radiatively (k_r) over the total absorbed photons. Essentially, ϕ_F determines the efficiency of the conversion of absorbed light into emitted light.¹¹

$$(9) \quad \phi_F = \frac{\text{emitted photons}}{\text{absorbed photons}} = \frac{k_r}{k_r + k_{ISC} + k_I}$$

Experimentally, the fluorescence quantum yield is measured by comparing the fluorescence intensity of the molecule with that of reference standard with a known quantum yield.

$$(10) \quad \phi_2 = \frac{OD_1 * \sum F_2}{OD_2 * \sum F_1} \phi_1$$

Where:

F_2 -fluorescence intensity of the molecule with unknown quantum yield,

F_1 -fluorescence intensity of the reference molecule with quantum yield ϕ_1 .

Therefore, in order to measure the quantum yield of a compound, one must measure the optical densities and fluorescence intensities of the fluorophore and reference compound under the same conditions and environment.

This method of determining the quantum yield using a reference compound is called the relative fluorescence quantum yield. Recently, absolute measurements of quantum yields can be done using stand-alone integrating sphere setups, which detect all light emitted by the excited molecule and measure the absolute fluorescence quantum yield by comparing the number of emitted photons with the number of absorbed photons.¹¹

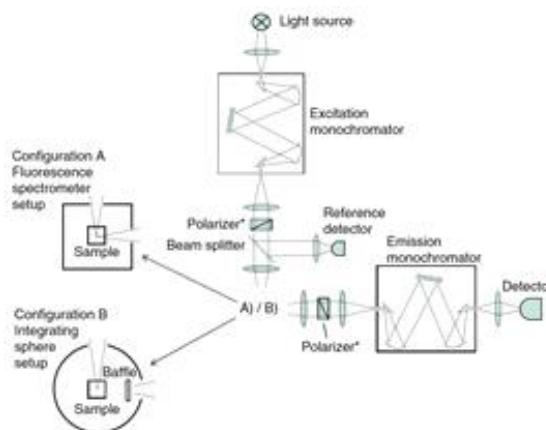


Figure 2. Instrumental setups of a fluorescence spectrometer (configuration A) and of an integrating sphere (configuration B). *Polarizers are not needed for an integrating sphere setup. Source: *Nature Protocols* volume 8, pages 1535-1550 (2013)

1.6. Fluorophore Structure and Properties

Fluorescent compounds can be divided into two categories: intrinsic and extrinsic probes. Intrinsic probes exist in nature and are sufficient to be of practical use. They include aromatic amino acids such as tyrosine and tryptophan, NADH, FAD, FMD, phosphate, chlorophylls, pteridines, among others.² Extrinsic probes, on the other hand, can form a covalent or noncovalent complex with the target system. Some examples of extrinsic probes are dansyl chloride, Hoechst dyes, ethidium bromide, iodoacetamide, maleimide and several others. Presently, thousands of fluorescent compounds are synthesized and several of them are commercially available for various applications.

The relationship between molecular structure and fluorescent properties has been recognized and used to synthesize fluorophores. Fluorescence is generally observed in molecules with $\pi \rightarrow \pi^*$ as their lowest energy transition, such as aromatic compounds. Several aliphatic, alicyclic carbonyl and highly conjugated double bond structures exhibit fluorescence as well. In addition, rigidity is another structural feature associated high fluorescence quantum yields. Rigid molecules have less intramolecular thermal motion, which deactivates excited states non-radiatively leading to a reduction in fluorescence intensity.¹² This reduction in fluorescence intensity due non-radiative

pathways caused by the energy-absorbing flexible group is aptly called the "loose-bolt effect" or "loose-bolt theory".¹³

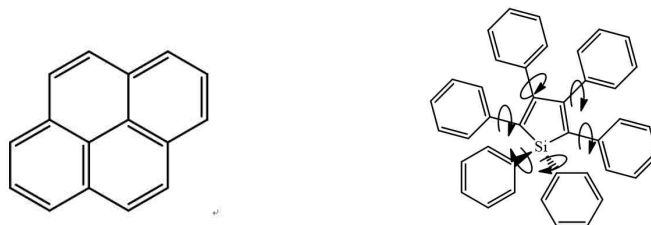


Figure 3. Pyrene (left), an example of a rigid fluorophore and hexaphenylsilole (right), an AIE molecule.

However, this same structural feature has been put to good use with the advent of the aggregation-induced emission (AIE). Due to the extensive conjugation, most fluorophores are hydrophobic and therefore, form non-fluorescent aggregates in aqueous media. Planar luminogens such as pyrene aggregate due to δ - δ stacking interaction. Upon aggregation, the excited states generally decay *via* non-radiative pathways, effectively quenching emission. This behavior is called aggregation-caused quenching (ACQ) of light emission. Several synthetic strategies has been reported to mitigate this problem such as introducing branched chains, bulky groups and rigid scaffolds to act as "spacer" between dye cores.^{14,15}

AIE was first observed in a series of silole molecules that were non-luminescent in the solution state but emitted light upon aggregation in 2001.¹⁶ The mechanism behind this unusual phenomenon is not yet completely understood although restriction of intramolecular rotation (RIR), conformational planarization, J-aggregate formation, and twisted intramolecular charge transfer (TICT) were proposed and discussed.¹⁷ Several AIE molecules have rotatable aromatic groups whose molecular motions in solution dissipate the excited-state energy *via* non-radiative pathways, hence without fluorescence. Upon aggregation, the same molecular motions are restricted so de-excitation *via* fluorescence dominates.¹⁸

2. BODIPY

2.1.Synthesis and General Features

Currently, one of the most extensively studied dye is 4,4-difluoro-4-bora-3a,4a-diaza-*s*-indacene (BODIPY) due to its sharp

emission intensity peaks with high fluorescence quantum yields, insensitivity to the pH and polarity of their environment, stability in physiological conditions, non-toxicity and tunability of their photophysical characteristics.¹⁹ The BODIPY core consists of dipyrromethene complexed with a disubstituted boron, most commonly BF₂. BODIPY dyes are typically synthesized from pyrrole with either anhydride, acyl chloride or aldehyde, and from ketopyrroles.

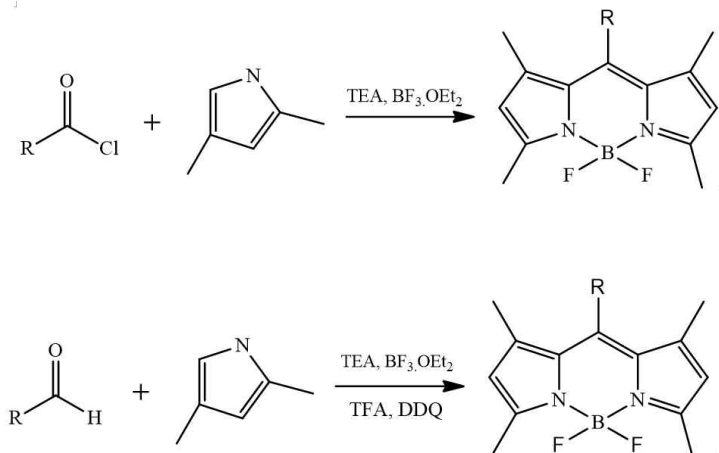


Figure 4. Typical synthetic schemes to afford BODIPY from acyl chloride and pyrrole (top), and from aldehyde and pyrrole (bottom).

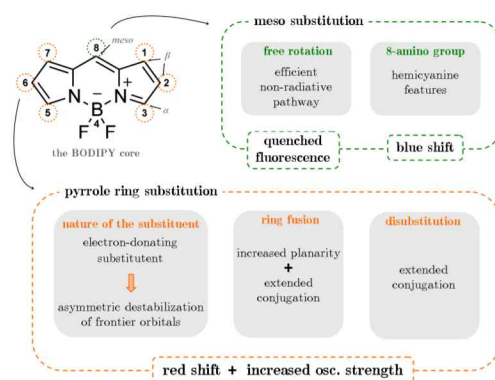


Figure 5. IUPAC numbering of BODIPY core structure and the primary results of modification. Source: Claire Tonnel' e. Chemical Sensors : Modelling the Photophysics of Cation Detection by Organic Dyes. Other. Universit' e Sciences et Technologies – Bordeaux I, 2013. English.²⁰

The ease of modification around the core is one of the favorable features of BODIPY. *De novo* approaches where the starting pyrrole already bear the functional groups and post-synthetic derivatization of the dye create a wide-array of BODIPY dyes with diverse characteristics. The meso- or 8-position can be replaced with a nitrogen atom to generate aza-BODIPY. Moreover, positions 1,2,3,5,6,7 in the pyrrole ring are sites of substitution and one or both of the fluorine atoms can be replaced with oxygen to bring about desired changes in the dye.

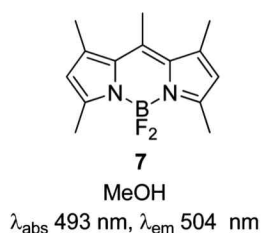


Figure 6. Structure of BODIPY and its corresponding absorbance and emission wavelength. Source: J. Phys. Chem. A 2012, 116, 9621–9631²¹

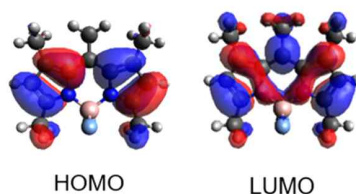


Figure 7. DFT HOMO and LUMO of BODIPY. Source: ACS Appl. Mater. Interfaces 2018, 10, 23254–23262

On a molecular-level, density functional theory (DFT) calculations on the structure of BODIPY reveal that the HOMO and LUMO are characterized as π -orbital. A nodal plane at the meso-position in the HOMO while a large molecular orbital coefficient is found in the same position in the LUMO, suggesting that substitution at the meso-position can tune the LUMO.²² Consistent with the large LUMO coefficient at the nitrogen atoms, complexation with boron trifluoride mostly affected the LUMO energy. In the HOMO, a nodal plane is found in the pyrrole nitrogen atoms. Aside from these, molecular orbital coefficients are predominantly larger in the HOMO than the LUMO, suggesting that attaching electron donating groups influences the HOMO more than the LUMO of the BODIPY.²³

These features have spurred the development of BODIPY dyes for bioimaging applications.

2.2. BODIPY dyes for bioimaging

Over the years, the demand for accurate and efficient detection and visualization of biomolecules have driven the development of fluorescence imaging technique and accordingly, the search for appropriate fluorescent probes. The most widely used and commercially available dyes are coumarin, fluorescein, BODIPY, rhodamine and cyanine dyes.^{24,25} However, among them, the relatively new BODIPY has been considered as a potential scaffold for fluorescent bioimaging because it possesses several characteristics ideal as fluorescent probe such as high fluorescence quantum yield, high photostability, non-toxicity and neutral total charge. The structure of BODIPY also allows for diverse modifications to enhance the properties of the dye.

Nonetheless, BODIPY dyes, like other conjugated molecules, are hydrophobic and predisposed to aggregate in subcellular structures. This drawback is circumvented by modifying the dye core with hydrophilic moieties. Conjugating sulfate, phosphate and ammonium ions enhanced the solubility of the dye.²⁶ However, the presence of charges in these ionic groups may cause unwanted interactions with biomolecules so neutral substituents such as poly(ethylene glycol) chains are also preferred.^{27,28}

On the other hand, these bulky chains (PEG) can increase the particle size of the fluorophore and reduce its cell permeability. Solubilizing groups can even account for > 80% of the total molecular weight.²⁷ Hence, relatively small di/mono-alkoxy and di/mono-acetoxy BODIPYs that exhibit balance between aqueous solubility and lipophilicity to enable cell permeation without random staining of lipid membranes were also explored for cell imaging.²⁹ Reported di/mono-alkoxy and di/mono-acetoxy BODIPY dyes are accessed by substituting one or two of the fluorine atoms with suitable alcohols. Moreover, results from these researches suggest that substitution of the F atoms has little effect on the photophysical properties (absorption and emission wavelengths) of the dye although electron-donating groups diminish the fluorescence quantum yield while the opposite is observed with electron-withdrawing groups.³⁰⁻³²

A newer method of imparting solubility into the BODIPY is by using simple sugars such as lactose, glucose and galactose. In addition, these sugars can also act as targeting moieties of the dye. Lactose has been found to selectively target galectin-1, a beta-galactosidase-binding lectin whose over-expression is linked with breast cancer.³¹ On the other hand, glycoconjugation wherein glucose is attached to anticancer agents and drugs is based on the observation that cancerous tissues consume lots of glucose (called Warburg effect).³² Lastly, galactose can be used as a broad tumor ligand for targeted cancer therapy.³³ Considering the above

discussion, the applicability of glucose-conjugated BODIPY dyes has been extended to photodynamic therapy (PDT) and acted on human lung cancer A459 cell line.³⁴

Although the modification strategies mentioned previously are effective in imparting aqueous solubility, some BODIPY can be made more biocompatible by being encapsulated within nanocarriers. These structures self-assemble in water and dissociate in the target environment. This transition is accompanied by changes in emission intensity where encapsulated dyes fluoresce weakly due to aggregation but show strong emission once exposed. In this way, the dyes can be made photostable and resistant to photobleaching due to reduced interaction with reactive oxygen molecules.³⁵⁻³⁷

More specific-targeting BODIPY dyes are also made available by using sensitive and selective moieties. Positively charged molecules such as ammonium or phosphonium groups are usually used for mitochondria-targeting fluorescent probes.⁴⁰⁻⁴² These cations can localize in the negatively-charged mitochondria and can be used to further understand biological events in the organelle.

Cell matrix conditions, such as pH, can also be used to control the localization of the dyes such as BODIPY dyes with weakly basic targeting groups.⁴³⁻⁴⁶ Although cytoplasmic pH is maintained at neutral level, pH levels in endosomes, lysosomes and a few tumor tissues are fairly acidic.

Furthermore, BODIPYs modified with receptor ligands can selectively bind to proteins and hence, visualize the protein of interest.⁴⁷⁻⁵⁰ BODIPY FL-labeled fluorescent probe can target ERR α (Estrogen-related receptor alpha), an orphan nuclear receptor that is predominantly active in tissues with high metabolic needs and plays an important role in regulating gene expressions used in metabolism.⁵¹

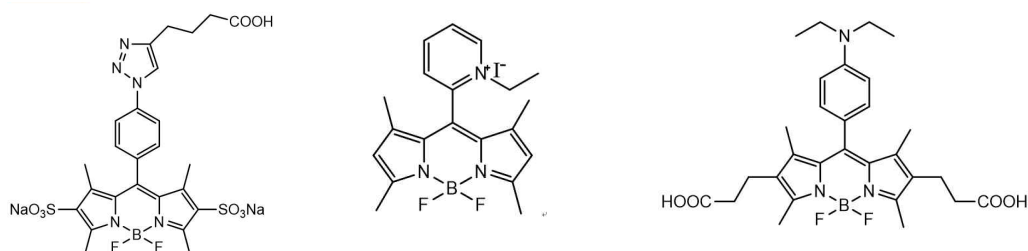


Figure 8. Some representative structures of water-soluble BODIPY (left), BODIPY with a mitochondria-targeting group (middle) and a pH-sensitive BODIPY dye.

2.3. Near-infrared BODIPY dyes

Recent years have seen the development of near-infrared (NIR) emitting fluorescent dyes. The advantages of NIR emitting dyes such as improved sensitivity, high contrast with low background noise, deep tissue penetration and less cell damage prompted the interest for novel NIR fluorophores with enhanced characteristics.⁵² Ideally, NIR dyes should absorb and emit within the biological window (650–900 nm), possess high fluorescence quantum yield, narrow excitation/emission, are photostable, have no or negligible toxicity and are biocompatible.⁵³ Pristine BODIPY, as well as fluorescein, rhodamine, cyanine and Nile red dyes, absorb and emit in the visible spectral region, well below the required wavelength range. Fortunately, NIR dyes are obtained by extending the δ -conjugation within the structure through aromatic ring incorporation, ethynylaryl substitution, aza-substitution at the meso-position and styryl modification.⁵⁴

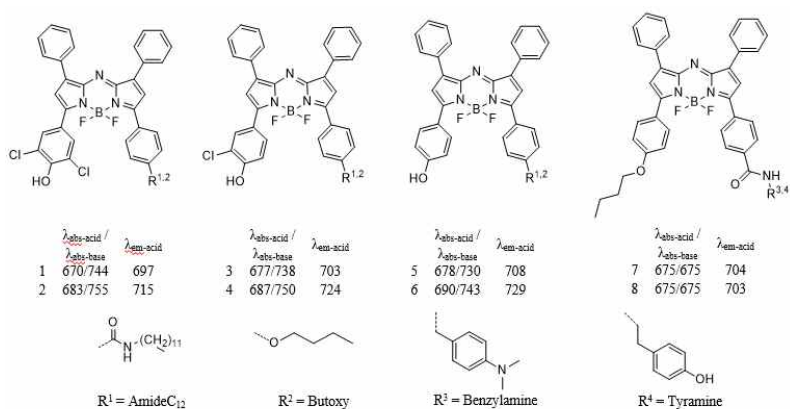
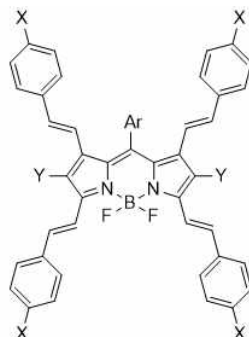


Figure 9. Aza-BODIPY dyes as NIR emitting dyes



Ar = 3,5-didecyloxyphenyl		λ_{abs} (nm)	λ_{em} (nm)
1 = OCH ₃	Y = Br	700	727
2 = OCH ₃	Y =	721	747
3 = OCH ₃	Y =	732	756
4 = N(CH ₃) ₂	Y =	802	837
5 = N(CH ₃) ₂	Y =	797	835

Figure 10. NIR emitting di-styryl modified BODIPY dyes with different substituents.

2.4. Other BODIPY dyes with enhanced photophysical properties

Although great progress has been made in synthesizing NIR-absorbing and selective BODIPY based fluorophores, upon *in vivo* applications, BODIPY dyes are still beset with problems in interacting with the physiological environment. Hence, other BODIPY dyes have emerged with enhanced properties.

2.4.1. Large Stokes shift and BODIPY fluorophores

A common problem with some fluorophores, e.g. fluorescein, rhodamine, oxazine, cyanine, are their small Stokes shifts - generally less than 30 nm.⁵⁵ BODIPY is no exception, with commercial dyes BODIPY 493/503 and 505/515 having a Stokes shift of 10 nm. As explained earlier, Stokes shift is an inherent feature of a specific compound. Small Stokes shifts pose a problem with inner-filter effects, poor signal-to-noise ratio and self-quenching due to self-absorption, even at low concentrations. Moreover, fluorophores with large Stokes shift are advantageous for exact imaging and sensing.⁵⁶ Attaining large Stokes-shifted fluorophores

can be done through a) excited state intramolecular charge transfer (ICT) between donor and acceptor moieties, b) twisted intermolecular charge transfer (TICT) and c) proton transfer, among others.⁵⁷⁻⁵⁹

Experimentally, a general strategy to achieve large Stokes-shifted fluorophores involving the introduction of vibronic structures has been proposed. This design is based on breaking the symmetric structures of most fluorescent dyes. Although symmetry throughout the HOMO and LUMO endowed fluorophores with high fluorescence quantum yields, this also brought about the weakening of vibrational sub-orbitals. Consequently, excited-state electrons fail to interconvert to lower vibrational states, making the excitation and emission wavelength close to each other. With the introduction of asymmetric structures, vibronic contributions to the HOMO and LUMO can induced efficient internal conversion of the excited-state electrons to lower vibrational states. This then will reduce emission energy and increase the Stokes shift of the fluorophore.⁵⁶ For example, 2-(thiophen-2-yl)quinoline appended BODIPY dye with styryl moieties at 1-,3-,5-,7- positions have displayed a large pseudo Stokes' shift of up to 400 nm. This is attributed to the efficient through-bond energy transfer in the nearly planar BODIPY dye.⁶⁰ Moreover, a library of asymmetric BODIPY dyes with styryl and carboxylic groups attached to the core exhibited controllable large Stokes' shift ranging from 10 to 51 nm. Steric hindrance and resonance effects have also contributed to the spectral changes.⁶¹

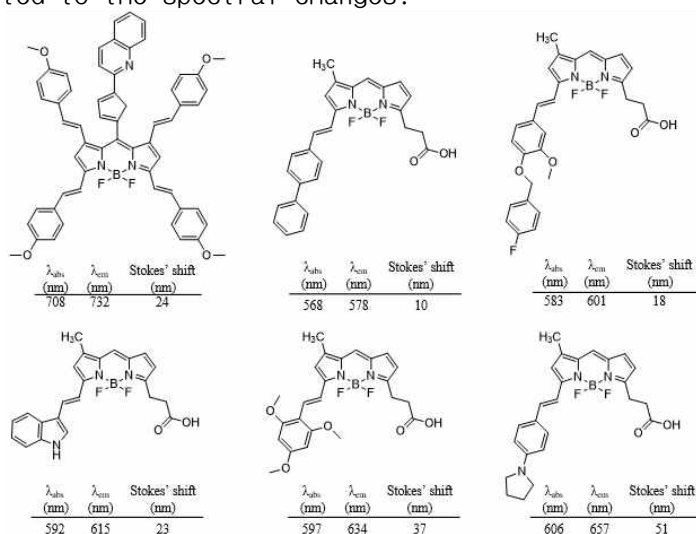


Figure 11. Changes in the Stokes' shift with different substitution patterns.

CHAPTER 2: Synthesis and Photophysical Characterization of Highly Water-Soluble PEGylated BODIPY Derivatives for Cellular Imaging

1. Introduction

Over the last decade, fluorescence imaging techniques have proved to be powerful tools for visualizing cell biology at many levels and for revealing spatiotemporal details about cellular dynamics.⁶²⁻⁶⁵ They have paved the way for the development of various fluorescent probes, including fluorescent proteins, nanocrystals (quantum dots), and small organic fluorescent dyes, to provide highly sensitive, minimally invasive, and safe detection of cells and tissues.^{63,66} However, such fluorescent systems often suffer from several shortcomings which impede their potential application as biological probes. In particular, organic dyes commonly suffer from aggregation-caused fluorescence quenching (ACQ) originating from the formation of non-emissive excimers or energy transfer to quenching sites.⁶⁷ To avoid the undesirable quenching effects, bulky protective groups have frequently been introduced to the periphery of the fluorescent core. By this approach, high fluorescence efficiencies can be retained in concentrated solutions, because the sterically bulky protective substituents can prevent intermolecular interactions and unfavorable aggregation.

Among the various organic fluorophores available, 4,4'-difluoro-4-bora-3a,4a-diaza-s-indacene (BODIPY) and its derivatives are widely used due to their sharp fluorescence emissions, large fluorescence quantum yields (QYs ; generally > 0.5), high molar extinction coefficients (typically > 80,000 L (mol · cm)⁻¹), modifiability, neutral total charges, and excellent photostability.^{36,42,68,69} Although BODIPY and its derivatives have been employed for fluorescence imaging studies, a vast majority of the research concerning the photophysical and electrochemical properties of BODIPY has been carried out in organic environments, whereas counterpart studies conducted in aqueous media are scarce.⁷⁰ Various bio-imaging BODIPY dyes have been reported, however they would accumulate in endoplasmic reticulum, mitochondria and subcellular membranes because of their lipophilicity, rigidity and total charge.^{68,71-73} Hence, it is of paramount importance to develop BODIPY dyes that are relatively water-soluble under physiological conditions and resist the formation of non-fluorescent aggregates, thereby being suitable for biological and medical use.³⁹ Appending hydrophilic moieties, such as poly(ethylene glycol) (PEG), *N,N*-bis(2-hydroxyethyl) amine, carbohydrates, nucleotides, or ionic groups like carboxylic acids, sulfonic acids, or

ammonium groups, to the BODIPY core are some of the approaches recently used to synthesize water-soluble BODIPY dyes.^{39,74-78}

Neutral water-soluble BODIPY dyes, such as PEGylated BODIPY, have an advantage over ionic dyes in that they avoid potential electrostatic interactions between the dyes and biomolecules in biological and medical applications.⁷⁹ Thus, the use of PEG to increase the water solubility of BODIPY dyes is a technique still widely used among researchers. It is also well known that PEG possesses several biological and medical advantages such as long circulation time, satisfactory biocompatibility, and a tendency to accumulate in tumor sites via the enhanced permeability and retention (EPR) effect of leaky tumor neovasculature.⁸⁰ Previous methods for introducing PEG chains as hydrophilic groups to the BODIPY core often involved arylation at the *meso* position of the dye core. This modification would result in an appreciable decrease in the fluorescence QY due to the free rotation of the *meso* substituent, causing energy losses via nonradiative deactivation of excited states.^{12,19} In light of the above discussion, we designed a facile synthetic route to prepare highly water-soluble PEGylated BODIPY dyes. Bulky di-branched PEG chains were prepared and introduced at the *meso* position of the BODIPY core, without the incorporation of a rotationally free phenyl ring. We investigated the optical properties and fluorescence quantum yields of the resultant dyes in both organic and aqueous solutions. The BODIPY dyes were well-distributed in the cellular cytoplasm area, wherein they exhibited high fluorescence intensity and low cytotoxicity, and are thus quite promising as bio-imaging agents.

2. Experimental

All reagents were obtained from commercial sources and were used without further purification unless specifically mentioned. 2,4-dimethyl-3-ethylpyrrole, 2,4-dimethylpyrrole, polyethylene glycol monomethyl ether (MPEG, $M_n = 350 \text{ g mol}^{-1}$), 3,5-dihydroxybenzoic acid and boron trifluoride diethyl etherate were purchased from Sigma-Aldrich Chemical Company (St. Louis, MO, USA). 5-Bromovaleryl chloride was obtained from Tokyo Chemical Industry (Tokyo, Japan). Tetrabutylammonium bromide was obtained from Junsei Chemical Co., Ltd. (Tokyo, Japan). Triethylamine and tosyl chloride were bought from Daejung Chemicals & Metals Co., Ltd. (Siheung, South Korea). Solvents used were of analytical grade and purified using standard techniques. Thin layer chromatography was performed on precoated TLC plates from Merck (Silica Gel 60 F254). NMR Spectroscopic data were obtained from the Korea Basic Science Institute, Gwangju branch. ^1H and ^{13}C NMR spectra were referenced to the residual proton resonance of CDCl_3 ($\delta 7.26$) and recorded on a JEOL JNM-AL300 spectrometer (Japan) with tetramethylsilane (TMS) as the

internal standard. ^{11}B (400MHz) NMR spectra were referenced to $\text{BF}_3\text{Et}_2\text{O}$. ^{19}F (500MHz) NMR chemical shifts were calibrated using CF_3COOH as external standard. Absorption spectra were measured with Hitachi 5300 spectrophotometer from 200 to 900 nm using 10 mm quartz cuvette. Fluorescence emission intensities were measured with Hitachi F-7000 fluorescence spectrophotometer. Absolute fluorescence quantum yields were measured with Hamamatsu Photonics Quantarius - QY Absolute PL quantum yield spectrometer (Hamamatsu Photonics K.K., Hamamatsu, Japan). Cell images were captured using a Zeiss confocal laser scanning microscope. Bruker Ultraflex extreme MALDI-TOF/TOF mass spectrometer (Berlin, Germany) at the Ochang Branch of the Korean Basic Science Institute was used to measure the mass of the final compounds.

2.1. Synthesis of halogenated dyes

2.1.1 BODIPY-(CH₂)₄-Br

The halogenated dye was prepared according to a previously published method.⁸¹ 5-Bromovaleryl chloride (0.352 ml, 1.00 eq) was added dropwise to a stirred solution of 2,4-dimethylpyrrole (0.500 g, 2.00 eq) in anhydrous dichloromethane at 50° C for 2 h. After the solvent was evaporated, the residual solid was dissolved in toluene (35 ml) and dichloromethane (15 ml). Triethylamine (1.54 ml, 4.20 eq) was added, and the mixture was stirred under argon atmosphere for 30 min, and then boron trifluoride diethyl etherate (1.62 ml, 5.00 eq) was added dropwise. The reaction mixture was refluxed for 1.5 h at 50° C and the solvent was vacuum evaporated. The crude product was purified by silica gel column chromatography eluting with CH_2Cl_2 -hexane. Yield 49%. ^1H NMR (CDCl_3 , 400MHz): δ = 6.07 (s, 2H), 3.46 (t, 2H), 2.99 (t, 2H), 2.52 (s, 6H), 2.43 (s, 6H), 2.06 (t, 2H), 1.82 (t, 2H) ppm.

2.1.2. Ethyl-BODIPY-(CH₂)₄-Br

This compound was prepared in the same way as BODIPY-(CH₂)₄-Br, using 2,4-dimethyl-3-ethylpyrrole (0.500 g, 2.00 eq). All other reagents were scaled accordingly. The crude product was purified by silica gel column chromatography eluting with CH_2Cl_2 -hexane. Yield 56%. ^1H NMR (CDCl_3 , 400MHz): δ = 3.46 (t, 2H), 3.03 (t, 2H), 2.50 (s, 6H), 2.41 (m, 4H), 2.35 (s, 6H), 2.07 (t, 2H), 1.83 (t, 2H), 1.05 (t, 6H) ppm.

2.2 Synthesis of Poly(ethyleneglycol)methyl ether tosylate

The PEG moiety was synthesized according to the previously reported procedure.⁸² Briefly, 350 MW monomethyl polyethylene glycol (5.00 g, 1.00 eq) was dissolved in 5.00 mL of anhydrous pyridine. Tosyl chloride (3.27 g, 1.20 eq) was dissolved in anhydrous methylene chloride and slowly injected into the solution. The solution was continuously stirred under Ar gas for 8 h at RT. Then, 6N HCl solution (5 times the total volume of pyridine used) was added into the solution. The mixture was extracted with dichloromethane three (3) times and the organic layer was washed with 2N HCl solution. After drying with MgSO₄, the solvent was evaporated to afford the tosylated PEG as a colorless oil. Yield 76%. ¹H NMR (CDCl₃, 400MHz) : δ=7.81 (d,2H), 7.36 (d,2H), 4.16 (t,2H), 3.68–3.61 (m,32H), 3.58 (t,2H), 3.38 (s,3H), 2.45 (s,3H) ppm.

2.3. Synthesis of Ethyl-3,5-dialkoxy benzoate

Ethyl-3,5-dihydroxy benzoate (0.636 g, 1.00 eq), PEG methyl ether tosylate (4.00 g, 2.2 eq) and anhydrous K₂CO₃ (2.12g,4.4eq) were dissolved in anhydrous DMF and the solution was refluxed for 12 h at 80° C under Ar atmosphere.⁸² Then, the solution was poured into ice-cold water and extracted with dichloromethane three (3) times. The organic layer was washed with water and brine, and dried over MgSO₄, following which the solvent was removed by rotary evaporation. The crude product was purified by silica gel column chromatography using CH₂Cl₂ and MeOH as eluent. Yield 53%. ¹H NMR (CDCl₃, 400MHz): δ = 7.20 (s,2H), 6.69 (s,1H), 4.37 (m,2H), 4.16 (t,4H), 3.76–3.60 (m,52H), 3.54 (t,4H), 3.38 (s,6H), 1.38 (t,3H) ppm.

2.4. Synthesis of 3,5-dialkoxy benzoic acid

In a THF-H₂O (1:1) mixed solvent system, ethyl-3,5-dialkoxy benzoate (3.47g,1.00eq) and sodium hydroxide (0.473g, 3.00 eq) were dissolved and refluxed for 24 h at 80° C. After the solution cools to room temperature, the pH was adjusted to 3–4 using 10% v/v HCl. Then it was extracted using CH₂Cl₂, dried over MgSO₄ and concentrated *via* rotary evaporation to afford a brown oil. Yield 13%. ¹H NMR (CDCl₃, 400MHz): δ = 7.25 (s,2H), 6.70 (s,2H), 4.16 (t,4H), 3.71–3.65 (m,52H), 3.57 (m,4H), 3.38 (s,6H) ppm.

2.5. Synthesis of PEGylated BODIPY

To KOH (5.00 mg, 1.00 eq) dissolved in MeOH, 3,5-dialkoxy benzoic acid (150 mg, 2.00 eq) was added and stirred. Then the solvent was completely removed to obtain potassium 3,5-dialkoxy benzoate. BODIPY-(CH₂)₄-Br (43.0 mg, 20 eq), potassium 3,5-dialkoxybenzoate (200 mg, 40 eq) and tetrabutylammonium bromide (1.81 mg, 1 eq) were dissolved in anhydrous DMF and refluxed at 40° C for 48h. After cooling to room temperature, the solvent was vacuum distilled, and the crude product was purified by silica gel column chromatography eluting with CH₂Cl₂: MeOH to afford **BOD-PEG** dye as a dark orange oil. Yield 17%. ¹H NMR (CDCl₃, 400 MHz): δ = 7.16 (d-s,2H), 6.69 (s,1H), 6.06 (s,2H), 4.36 (t,2H), 4.12 (t,4H), 3.69-3.64 (m,52H), 3.54 (t,4H), 3.38 (s,6H), 3.03 (m,2H), 2.51 (s,6H), 2.41 (s,6H), 1.96 (m,2H), 1.80 (m,2H) ppm. ¹³C NMR (CDCl₃, 300 MHz): δ 186.30, 177.96, 161.47, 160.01, 156.01, 135.43, 132.00, 130.11, 121.96, 108.13, 106.93, 101.70, 92.41, 72.02, 71.45, 70.92, 70.75, 70.66, 69.67, 67.78, 59.13, 42.78, 32.20, 29.74, 27.90, 16.39, 14.49. ¹⁹F NMR (CDCl₃, 500 MHz): δ = -147.10 (m) ppm. ¹¹B NMR (CDCl₃, 400 MHz): δ = 0.410 (t) ppm. MALDI-TOF/TOFMS: [M+Na]⁺ m/z: calculated for C₅₈H₉₅BF₂N₂NaO₂₀, 1211.64; found, 1213.713.

EtBOD-PEG was synthesized using the same procedure described above but with ethyl-BODIPY-(CH₂)₄-Br (40.0 mg, 1.00 eq). All the other reagents were scaled accordingly, and the crude product was purified by silica gel column chromatography eluting with CH₂Cl₂: MeOH to afford the PEGylated BODIPY as a dark magenta oil. Yield 25%. ¹H NMR (CDCl₃, 400 MHz): δ = 7.17 (d-s,2H), 6.70 (s,1H), 4.37 (t,2H), 4.12 (t,4H), 3.71-3.63 (m,52H), 3.56 (t,4H), 3.38 (s,6H), 3.07 (m,2H), 2.49 (s,6H), 2.40 (m,2H), 2.33 (s,6H), 2.05 (m,2H), 1.99 (t,2H), 1.03 (t,6H) ppm. ¹³C NMR (CDCl₃, 300 MHz): δ 187.42, 166.45, 160.02, 152.55, 144.06, 138.63, 135.75, 132.91, 132.06, 131.05, 108.18, 106.82, 100.06, 72.03, 71.46, 70.92, 70.76, 69.67, 67.78, 59.14, 42.79, 29.75, 29.18, 17.19, 16.09, 14.86, 13.37, 12.43. ¹⁹F NMR (CDCl₃, 500 MHz): δ = -146.43 (m) ppm. ¹¹B NMR (CDCl₃, 400MHz): δ = 0.458 (t) ppm. MALDI-TOF /TOFMS: [M+Na]⁺ m/z: calculated for C₆₂H₁₀₃BF₂N₂NaO₂₀, 1267.71; found, 1267.786.

2.6. Cell proliferation assay

The human breast MCF-7 cells (3 × 10³ cells/well) were seeded in 96-well plates. After the cells were maintained for 24 h, cells were treated with either **BOD-PEG** or **EtBOD-PEG** dye for 24 h. Cell proliferation assay was measured using CellTiter 96 @ AQueous One

Solution Cell Proliferation Assay (Promega, Madison, WI, USA) according to the manufacturer's instruction. This assay contains MTS[3-(4,5-dimethylthiazol-2-yl)-5-(3-carboxymethoxyphenyl)-2-(4-sulfophenyl)-2H-tetrazolium] which is reduced to formazan by the action of NADH or NADPH in metabolically active cells.⁸³ The absorbance value of the wells containing solutions of MTS (background) was subtracted from those of the wells containing the treated and control cells.

2.7. Confocal microscopy

MCF-7 cells were grown on sterilized coverslips in 12-well overnight and then treated with either BOD-PEG or EtBOD-PEG dye for 24 h. After washing with phosphate-buffered saline (PBS), cells were fixed with 4% paraformaldehyde for 60 min and permeabilized with 0.5% Triton X-100 for 10 mins at room temperature. The slides were mounted with Vectashield mounting medium with 4',6-Diamidino-2-phenylindole (DAPI) (Vector Laboratories, Burlingame, CA, USA) following the manufacturer's instructions. Images were captured with a confocal microscope at 20× magnification (LSM-700; Carl Zeiss Microimaging Inc., Stockholm, Sweden).

3. Results and Discussion

3.1. Synthesis of PEGylated BODIPY Dyes

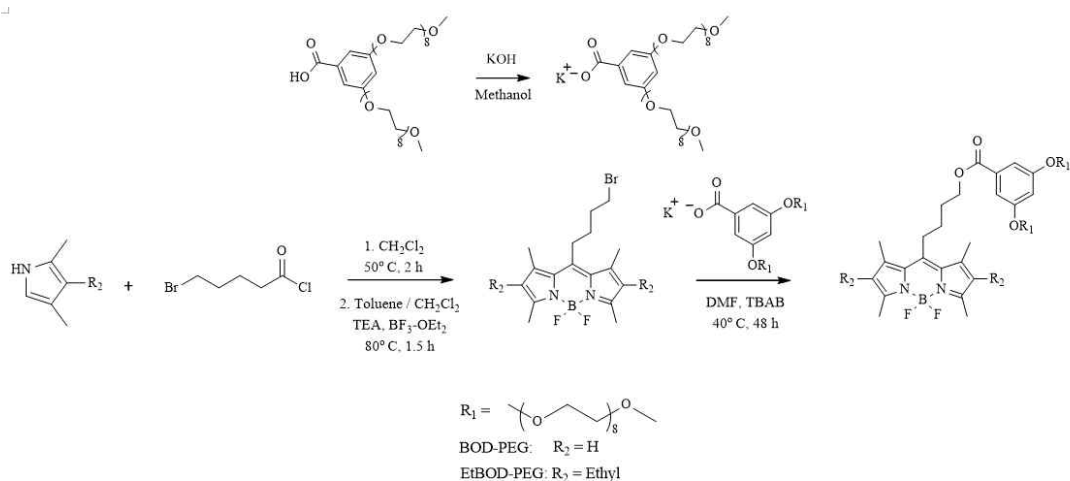


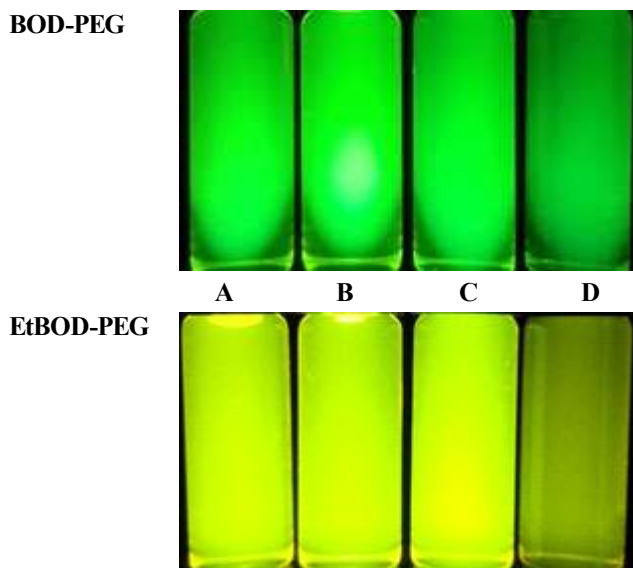
Figure 12. Synthesis of PEG-functionalized BODIPY fluorescent dyes BOD-PEG and EtBOD-PEG.

Figure 12 outlines the synthesis of the fluorescent BODIPY dyes containing di-branched PEG chains. The di-branched PEG chains were prepared according to previously reported methods.⁸² First, Williamson etherification between ethyl 3,5-dihydroxybenzoate and tosylated PEG produced di-PEGylated benzoates. Their subsequent hydrolysis yielded di-PEGylated benzoic acid. *Meso*-1-bromo-butyl-substituted BODIPY dyes were prepared via the condensation of 5-bromovaleryl chloride with either 2,4-dimethyl-3-ethylpyrrole or 2,4-dimethylpyrrole and subsequent complexation with $\text{BF}_3 \cdot \text{OEt}_2$ in the presence of triethylamine. Finally, the esterification between the bromine-containing BODIPYs and the carboxyl ends of the di-PEGylated benzoic acid afforded the water-soluble BODIPY dyes in moderate yields; 16.6% and 25.2% for **BOD-PEG** and **EtBOD-PEG**, respectively. The formation of an ester bond is evidenced by the appearance of triplet peaks at 4.36/4.37 ppm in the ^1H NMR spectra. All intermediate compounds were characterized by ^1H NMR, and the final products were also characterized by ^{13}C NMR, ^{19}F NMR and ^{11}B NMR. High-resolution mass spectrometry analysis showed the PEG chains to be approximately 6–8 units in length.

3.2. Photophysical properties

Dye	Solvent	$\lambda_{\text{abs}}/\text{nm}$	$\lambda_{\text{em}}/\text{nm}$	QY ^c
BOD-PEG ^a	THF	498	516	0.681
	CH_2Cl_2	500	517	0.663
	EtOH	498	515	0.668
	H_2O	496	511	0.512
EtBOD-PEG ^b	THF	522	541	0.659
	CH_2Cl_2	524	541	0.658
	EtOH	522	539	0.624
	H_2O	520	535	0.254

Table 1. Photophysical properties of BOD-PEG and EtBOD-PEG dyes in different solvents at room temperature (concentration = 17.2 μM). ^aFor ϕ_{fl} measurements, $\lambda_{\text{ex}} = 500$ nm. ^bFor ϕ_{fl} measurements, $\lambda_{\text{ex}} = 520$ nm. ^cQY = Absolute fluorescence quantum yield.



Picture 1. Photographs of BOD-PEG and EtBOD-PEG under UV illumination (365 nm) in different solvents: (A) THF; (B) CH_2Cl_2 ; (C) EtOH; (D) H_2O (concentration = 17.2 μM).

The photophysical properties of **BOD-PEG** and **EtBOD-PEG** were investigated in different solvents, and are summarized in **Table 1**. As depicted in **Figures 13** and **14**, narrow absorption spectra mirroring the respective emission spectra were recorded for both fluorescent dyes. The absorption and emission profiles correspond to those of typical BODIPY derivatives,⁸⁴ indicating that the appended PEG did not exert a significant effect on the photophysical properties of the dye in any of the solvents used in this study. The absorption spectra of **BOD-PEG** exhibited maximum intensity (λ_{ab}) at 498–500 nm in organic solvents and at 496 nm in water, due to the π - π^* transition of the BODIPY unit. The λ_{ab} generally blue-shifts with an increase in the polarity of the solvent, but only by a few nanometers. The emission peaks of **BOD-PEG** were observed at 515–517 nm in organic solvents and at 511 nm in water. The presence of ethyl groups at the 2,6 positions of the BODIPY core in the dye **EtBOD-PEG** resulted in red-shifts in the absorption spectra of ~20 nm relative to its unsubstituted counterpart (520–524 nm), to 539–541 nm in organic solvents and 535 nm in water. Theoretical studies have indicated that electron-withdrawing substituents stabilize the lowest unoccupied molecular orbital (LUMO) of BODIPY units, while electron-donating substituents destabilize the LUMO.^{85,86} Therefore, electron-donating ethyl

units resulted in the red-shifted emission of EtBOD-PEG relative to that of BOD-PEG.

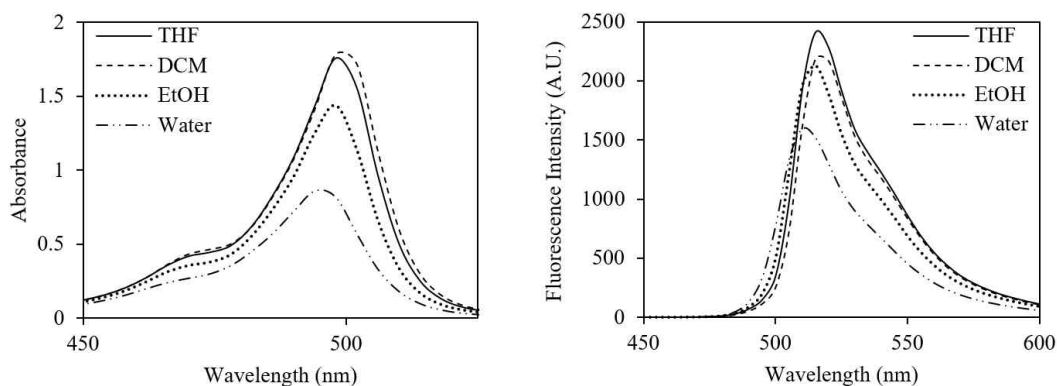


Figure 13. Absorption (left) and emission (right) spectra ($\lambda_{\text{ex}} = 496\text{--}500$ nm) of BOD-PEG dye in different solvents (concentration = $17.2 \mu\text{M}$).

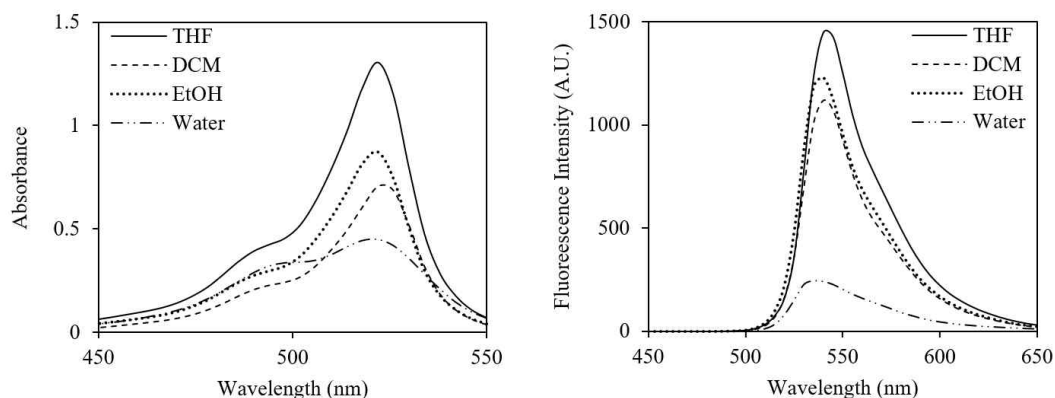


Figure 14. Absorption (left) and emission (right) spectra ($\lambda_{\text{ex}} = 520\text{--}524$ nm) of EtBOD-PEG dye in different solvents (concentration = $17.2 \mu\text{M}$).

In the case of EtBOD-PEG, broadening of the peak at 480–500 nm in the absorption profile in water seemed to suggest dye aggregation. To understand this behavior further, we studied the fluorescence spectra and fluorescence QY of both dyes in aqueous solution as a function of concentration, as depicted in **Figure 15**. The fluorescence spectra of BODIPY dyes were red-shifted by about 30 nm and the emission intensities decreased exponentially as the dye concentrations were increased from $1.0 \mu\text{M}$ to $10.0 \mu\text{M}$. This phenomenon may be ascribed to intermolecular interactions or aggregation in aqueous solution induced by the

increasing concentration of the dyes.⁸⁷ The QYs of the dyes in water at 1.0 μM reached 0.514 for **BOD-PEG** and 0.471 for **EtBOD-PEG**. At concentrations of 30.0 μM , the fluorescence QYs decreased to 0.361 for **BOD-PEG** and 0.138 for **EtBOD-PEG** (Table 2). Notably, both dyes exhibited relatively high fluorescence QYs even at concentrations of 30.0 μM , because the aggregation of the dyes in water was suppressed by the hydrophilic and sterically hindering groups. Further, relative to the unsubstituted **BOD-PEG**, the ethyl groups at the 2- and 6-positions in **EtBOD-PEG** increased the hydrophobic character of the dye core. In a study conducted by Nepomnyashchii *et al.*, 2,6-ethyl-substituted BODIPY dyes displayed lower fluorescence than their unsubstituted counterparts,⁷⁰ suggesting that hydrophobic interactions between the ethyl-substituted BODIPY dyes may play a role in this phenomenon.

Dye	Conc. (μM)	ϕ_{fl}
BOD-PEG ^a	1.0	0.514
	10.0	0.561
	30.0	0.361
EtBOD-PEG ^b	1.0	0.471
	10.0	0.292
	30.0	0.138

Table 2. Absolute fluorescence quantum yields of **BOD-PEG** and **EtBOD-PEG** dyes in water at different concentrations.

^a $\lambda_{ex} = 500 \text{ nm}$. ^b $\lambda_{ex} = 520 \text{ nm}$.

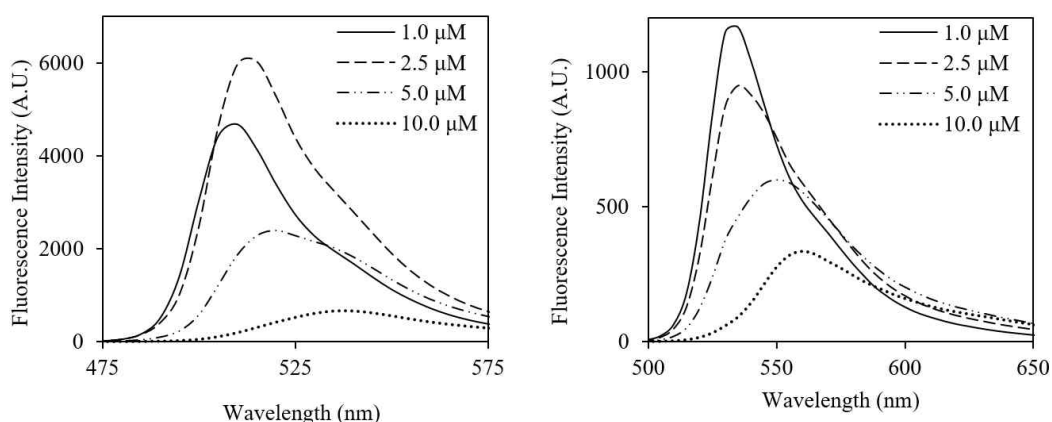


Figure 15. Emission spectra of **BOD-PEG** (left, $\lambda_{ex} = 506 \text{ nm}$) and **EtBOD-PEG** (right, $\lambda_{ex} = 530 \text{ nm}$) dyes in water at different concentrations.

3.3 Cell viability and imaging

One of the critical requirements for fluorescent probes is good biocompatibility.⁴² The CellTiter 96 ® AQueous One Solution Cell Proliferation Assay was used to assess the cytotoxicity of the BODIPY dyes. This method is based on the bioreduction of the tetrazolium compound MTS (Owen's reagent) to a colored formazan product by the cells. The quantity of formazan produced, as measured by absorbance at 490 nm, is directly proportional to the number of viable cells.⁸³ Cell viability experiments for the BODIPY dyes synthesized in this study were carried out employing MCF-7 human breast cancer cells. The test cells were incubated with either **BOD-PEG** or **EtBOD-PEG** dye at concentrations ranging from 2.5 to 10 μM . As shown in **Fig. 16**, there was no significant reduction in the viability of the cells after 24 h incubation with the fluorescent dyes. The BODIPY probes did not exhibit signs of toxicity towards the tested cells at low concentrations. Moreover, it is noteworthy that the number of living cells was maintained at approximately 90% and 80% of the original count for **BOD-PEG** and **EtBOD-PEG**, respectively, even after treatment with 10 μM of the dye. These results indicate that neither dye is significantly cytotoxic under the tested conditions over 24 h.

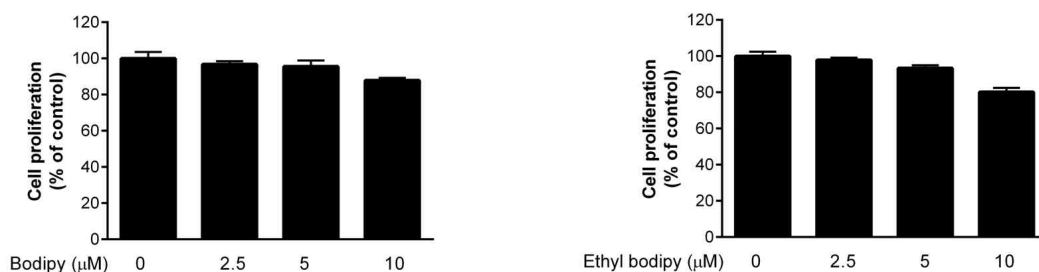
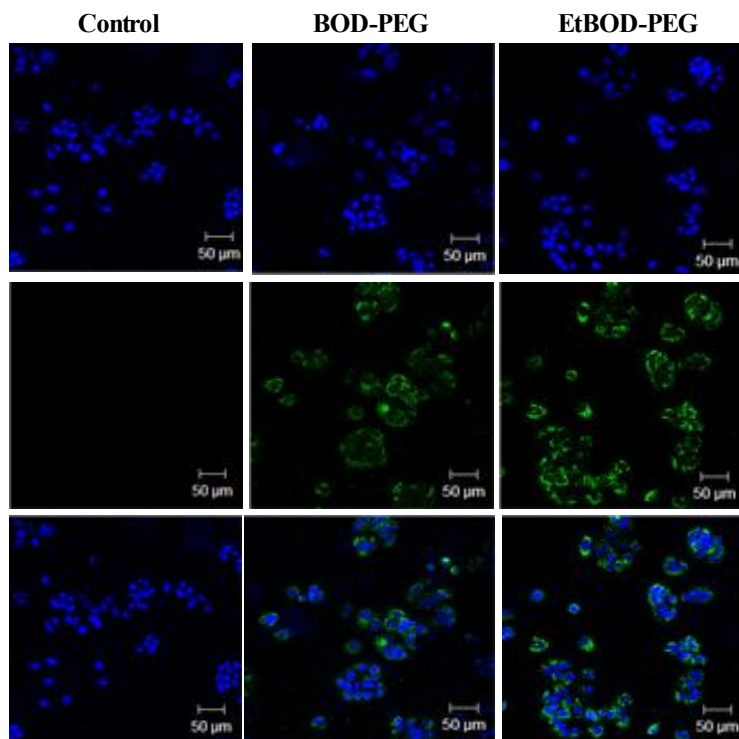


Figure 16. The relative number of viable cells after incubation with different concentrations of **BOD-PEG** (top) and **EtBOD-PEG** (bottom) dyes for 24 h.

To evaluate the potential application of the fluorescent dyes for bioimaging, MCF-7 cells were treated with the dyes for 24 h and imaged by confocal microscopy. 4',6-diamidino-2-phenylindole (DAPI), a fluorescent stain commonly used to visualize the nucleus, is employed to confirm the localization of the fluorescent dyes within the cells.⁸⁸ As shown in **Figure 17**, there was no fluorescence emission from the control untreated cells, while the test cells incubated with the dyes at concentrations of 10 μM emitted bright green fluorescence of high intensity. Additionally, the fluorescence microscopy images of the MCF-7

cells with the fluorescent probes showed that BODIPY dyes were successfully taken in by the cells, efficiently localized, and then fluoresced upon excitation.

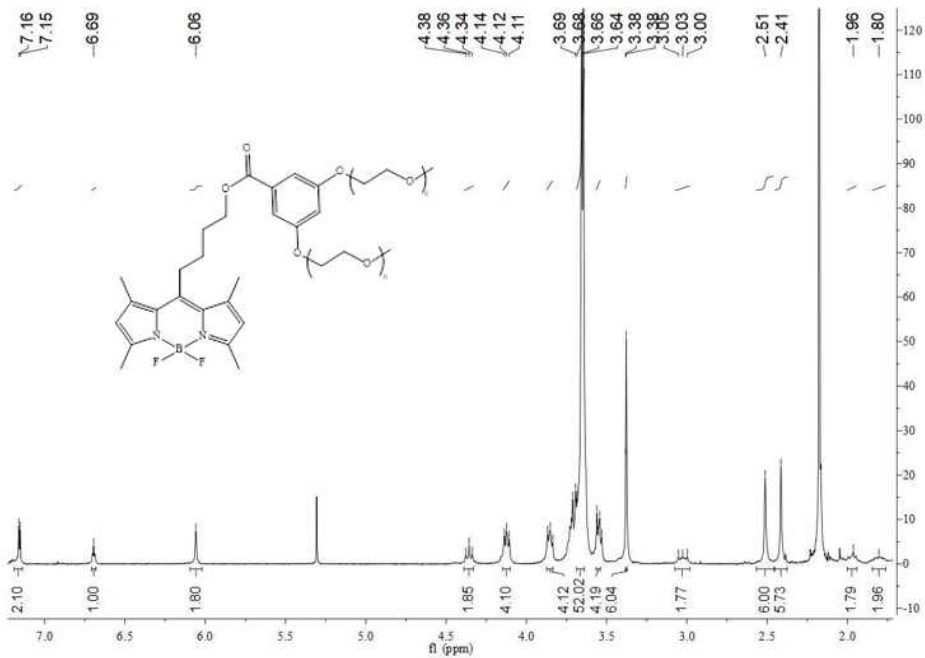


Picture 2. CLSM images of MCF-7 human breast cancer cells with either BOD-PEG or EtBOD-PEG dye at various concentrations, with the nucleus labeled with 4',6-diamidino-2-phenylindole (DAPI). Top: DAPI images; middle: BOD-PEG/ EtBOD-PEG dye images; bottom: merged images of both (concentration = 10.0 μM).

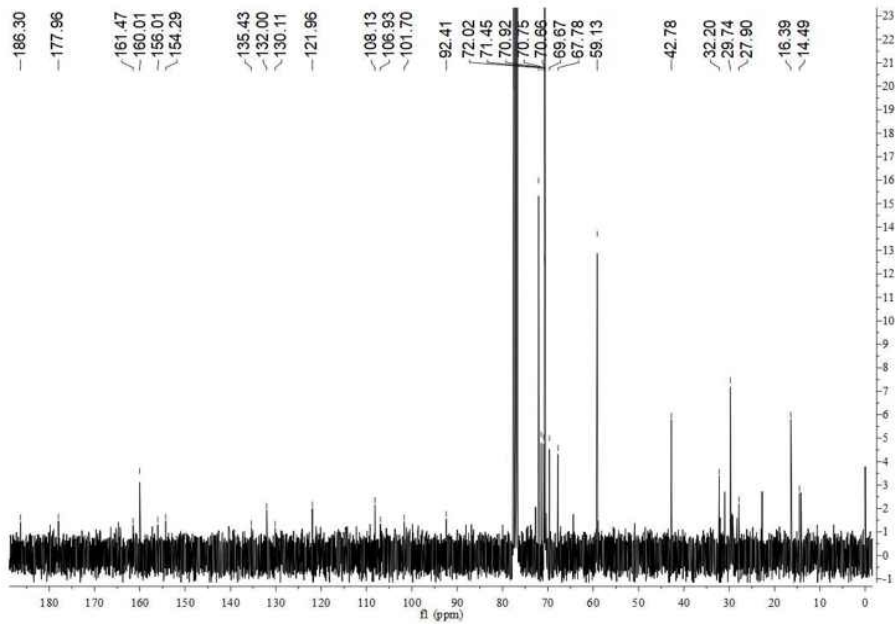
4. Conclusion

In this study, a series of water-soluble PEGylated BODIPY dyes (BOD-PEG and EtBOD-PEG) were prepared, and their photophysical properties were investigated. Bulky di-branched PEG chains were introduced at the *meso* position of the BODIPY core to reduce the aggregation tendencies of the dyes. The dye BOD-PEG, which has no substitutions at positions 2 and 6 of the BODIPY core, exhibited absorption and emission maxima at shorter wavelengths relative to those of EtBOD-PEG, which has electron-donating ethyl groups at the 2 and 6 positions of the core. Notably, the

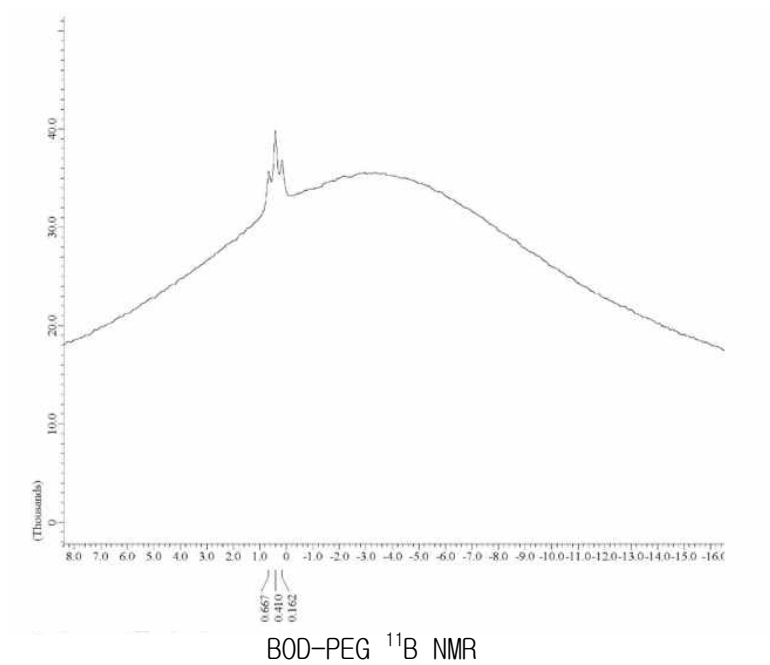
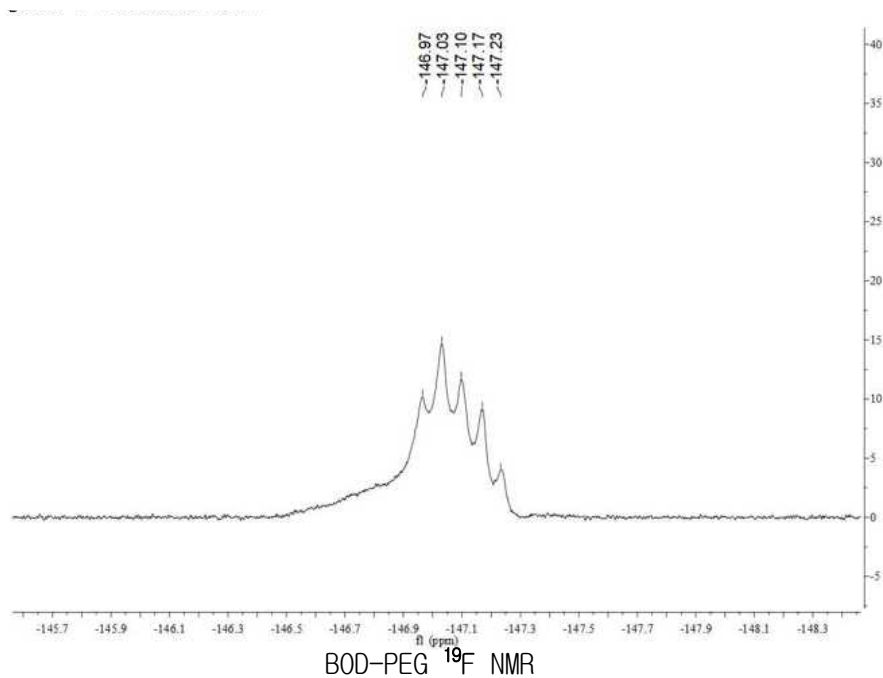
fluorescence QYs of the dyes at 1 μM in water were 0.514 for BOD-PEG and 0.471 for EtBOD-PEG, which are higher than those of other BODIPY-based water-soluble probes reported previously. The PEGylated BODIPY dyes were able to permeate MCF-7 cells and localized in the cellular cytoplasm, exhibiting good water solubility and biocompatibility. This work may provide new strategies for the design and fabrication of highly efficient fluorescent probes in aqueous environments.

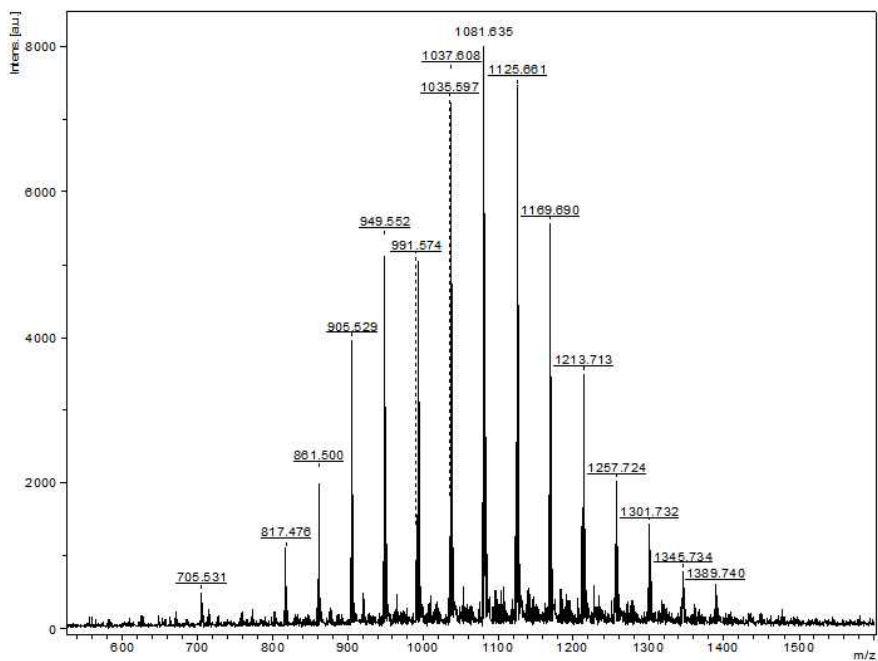


BOD-PEG

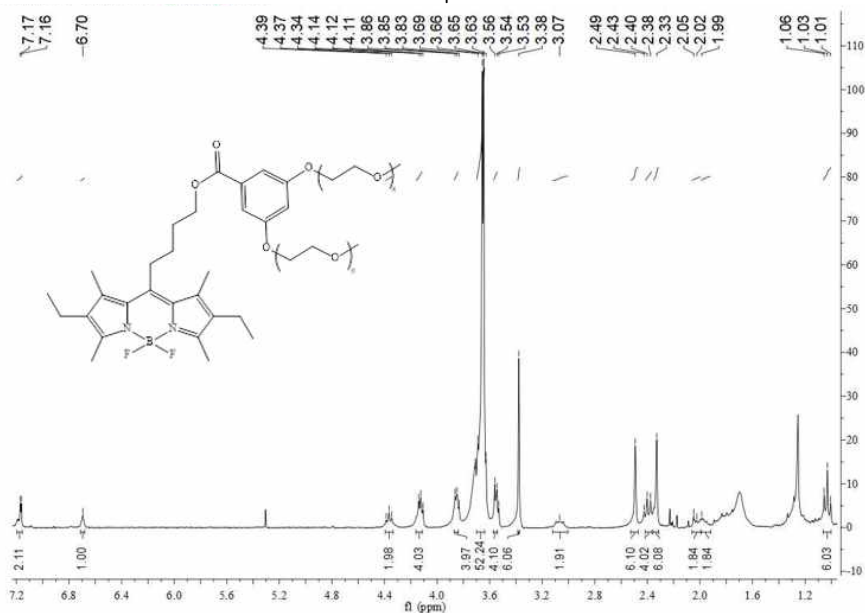


BOD-PEG- ^{13}C NMR

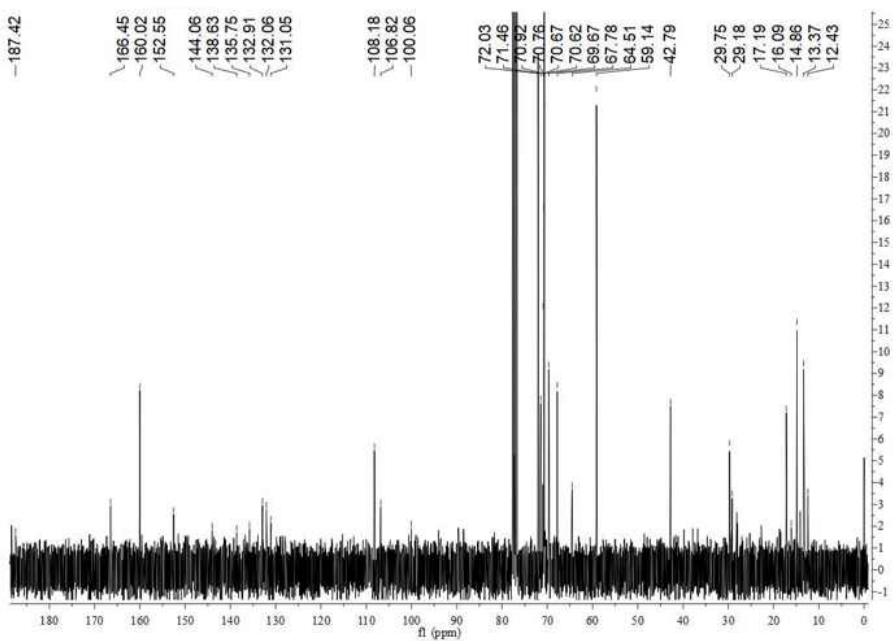




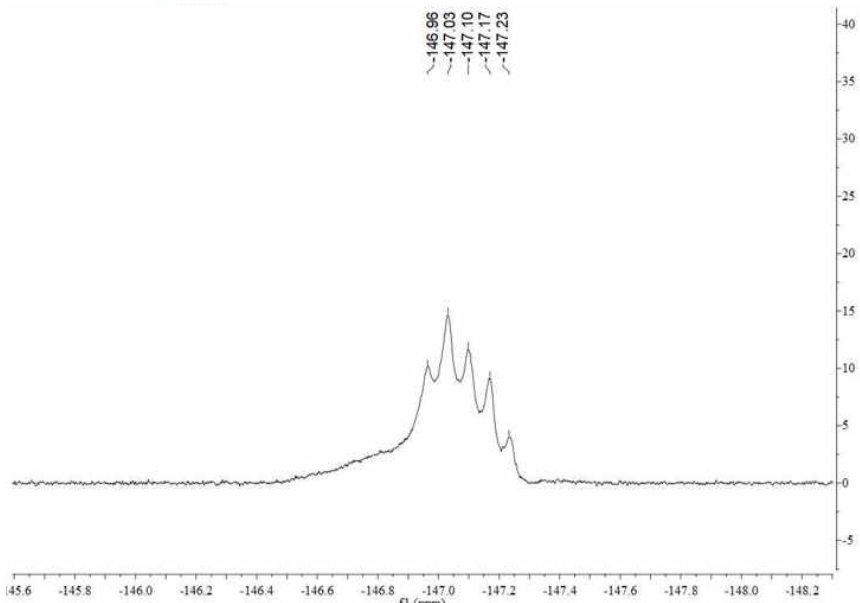
BOD-PEG MS spectrum



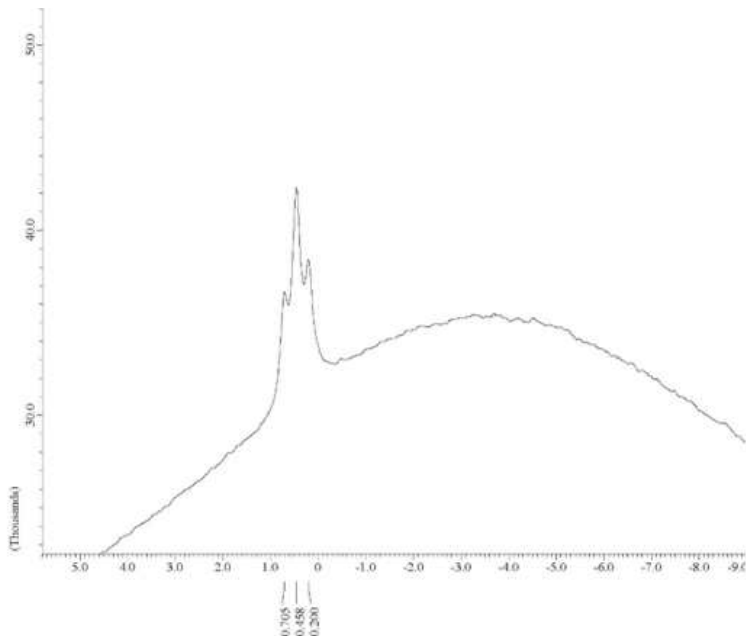
EtBOD-PEG



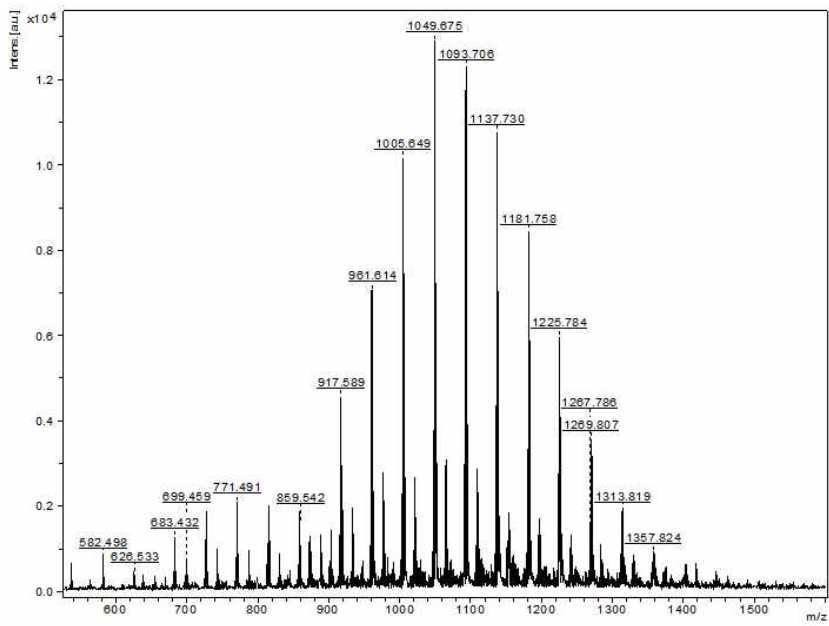
EtBOD-PEG ¹³C NMR



EtBOD-PEG ¹⁹F NMR



EtBOD-PEG ^{11}B NMR



EtBOD-PEG MS spectrum

devices.^{101,102} An IPN consists of two or more interlaced polymers that are not covalently bonded to each other. Therefore, by controlling the polymer composition and crosslinking method, the properties of the IPN structures can be tailored to obtain the desired features.^{98,103} Especially, chitosans have been combined with specific stimuli-responsive polymers in IPN structures to make them enzyme-, pH-, and temperature sensitive.¹⁰⁴ The chitosan-based IPNs have been found to be suitable for drug-delivery systems and tissue-engineering hydrogels because of their excellent biocompatibility, biodegradability, and facile synthesis.^{105,106}

In this study, multi-responsive hydrogels have been prepared using chitosan-based IPN structures. The pre-formed poly(hydroxyethyl methacrylate) (pHEMA) hydrogels were modified with chitosan-IPN structures which were newly synthesized using methacrylamide chitosan polymers. The subsequent functionalization with SP derivatives produced photochromic hydrogels and their photophysical properties such as color, absorption, and fluorescence were investigated upon exposure to specific illuminating sources and acid/base gases. Attaching spiropyran on the surface of the IPN hydrogel ensures maximum exposure to the stimuli and provides enough space for the reversible spiropyran-merocyanine molecular switch.

2. Experimental

2-Hydroxyethyl methacrylate (HEMA) was purchased from Junsei (Japan). Ethylene glycol dimethacrylate (EGDMA), Azobisisobutyronitrile (AIBN), and ammonium persulfate (APS) were acquired from Sigma-Aldrich. 1-ethyl-3-(3-dimethylaminopropyl)-carbodiimide hydrochloric acid (EDC.HCl) and sodium metabisulfite (SMBS) were sourced from Daejung. N-hydroxysuccinimide (NHS) and methacrylic anhydride were purchased from Alfa Aesar. Chitosan (600-800 kDa) was procured from Acros Organics (Geel, Belgium). Concentrated hydrochloric acid, ammonia solution (7 N in methanol), dimethylformamide (DMF), tetrahydrofuran (THF), chloroform, and other reagents were of analytical grade and used without further purification. Methacrylamide chitosan and carboxylic acid containing SP (SP-COOH) were synthesized according to previously reported procedures.^{90,107} The absorbance and fluorescence of the hydrogels was determined by using the Shimadzu UV-1650 PC (Japan) spectrophotometer and the Hitachi F-7000 fluorescence spectrophotometer, respectively. The hydrogels were illuminated with UV-light at 365 nm (UV-Model LV, France; 8 mW cm⁻²) or white LED light (SM 400-1, Korea; 48W).

2.1 Synthesis of SP-functionalized IPN Hydrogel

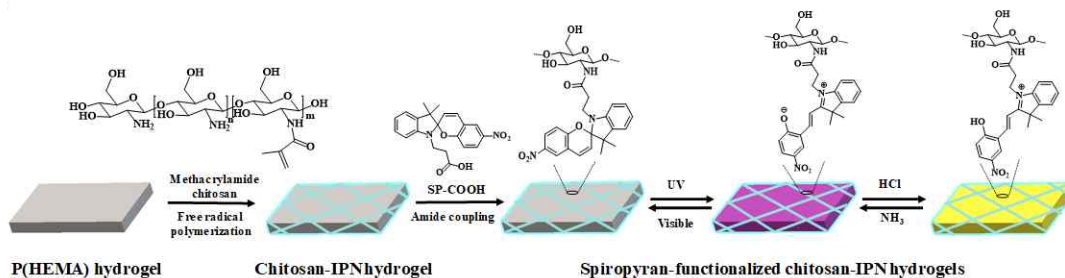


Figure 18. Preparation of SP-functionalized chitosan-IPN hydrogels and the structural conversion of SP with light and gases.

EGDMA (0.04 g) and a small amount of azobisisobutyronitrile were dissolved in HEMA (9.92 g). The solution was sonicated for 10 min and transferred to a square mold made of two glass plates covered internally with a polypropylene sheet. The molds were exposed to UV light for 30 min and heated at 80 ° C for at least 4 h. Subsequently, the samples were removed from the molds and soaked in distilled water for 2 days to remove any unreacted reagents. After drying overnight at 40 ° C, they were immersed in a solution of methacrylamide chitosan in distilled water (2 w/v %) for 24 h. The samples were then washed with distilled water and immersed in 10 mL of a solution of APS (5 mg) and SMBS (5 mg) for 24 h. The hydrogels were washed with distilled water and immersed in THF with EDC, NHS, and SP-COOH for 24 h. Finally, they were washed with ethanol and distilled water for 2 days to remove any unreacted chemicals prior to characterization and to allow swelling, which facilitated cutting.¹⁰⁸ The resulting hydrogels were cut into 1×1 cm samples.

2.2 Isomerization of spiropyran in response to illumination and acid/base gas treatment

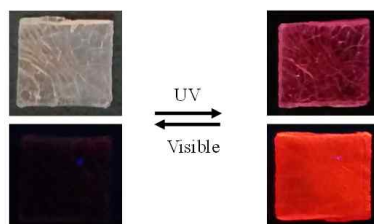
The hydrogels were illuminated either with white LED light for a minute or UV-light at 365 nm for three minutes to evaluate their photochromic ability. The portable light source was held 5 cm above the hydrogels. To observe their response to acid and base treatment, the purple hydrogels were placed in such a way that they completely covered the opening of the vials containing 4 mL of conc. hydrochloric acid (3 min) and 7 M ammonia in methanol solution (5 min), respectively.

3. Results and discussion

The multi-responsive hydrogels were prepared according to the synthetic scheme shown in Figure 18. In the first step, p(HEMA)-based hydrogels were prepared via radical polymerization using HEMA monomer with EGDMA as a cross-linker. In the second step, the resulting p(HEMA)-based hydrogels were interpenetrated with the methacrylamide chitosan polymer, and subsequent radical polymerization between chitosan backbones resulted in the chitosan-IPN structures consisting of cross-linked chitosan and p(HEMA) networks. Finally, the chitosan-IPN structures were covalently modified with SP molecules to form the multi-stimuli responsive hydrogels. Since natural chitosan is usually soluble in acidic conditions, it must be chemically modified to increase its solubility in neutral aqueous media or common organic solvents to be employed for the construction of chitosan-IPN structures.¹⁰⁶ Herein, we introduced methacrylate functionalities onto the chitosan polymers, giving rise to a methacrylamide chitosan.¹⁰⁷ The degree of methacryl modification was calculated to be 67.48%, based on the integrated area of the H2-H6 peaks observed in the range of 2.8-4.0 ppm and the methylene peaks at 5.2 and 5.6 ppm. Notably, methacrylamide chitosan contains considerable amounts of amine groups within its backbones. The p(HEMA) hydrogel modified with chitosan-IPN structures (**C-IPN-H**) was functionalized with SP-COOH via amide coupling between the primary amines in the chitosan backbones and the carboxylic acid groups of SP-COOH, resulting in the desired SP-functionalized hydrogel (**SP-IPN-H**).

To quantify the amount of SP molecules on the resultant hydrogels, UV/Vis absorption measurements were carried out using a standard calibration curve based on free SP-COOH in solution in a concentration range of 0.1 to 0.4 mM. Using Beer's Law and performing linear regression at 336 nm, the quantity of SP molecules incorporated on the hydrogel surface was estimated to be $0.140 \pm 0.0196 \mu\text{mol}/\text{cm}^2$. UV/Vis absorption and emission spectra were measured to investigate the photochromic properties in response to exposure to UV/Vis irradiation. The SP-modified hydrogel showed a strong absorption band in the range of 200 to 380 nm before exposure to UV radiation, while no absorbance was detected above 450 nm. This was attributed to the ring-closed SP form, which was predominant in the hydrogels. Upon UV-irradiation at 365 nm for 3 min, the SP-modified hydrogels changed from colorless to purple. Meanwhile, a new absorption band centered at 550 nm emerged because of the formation of the ring-open MC isomer with larger π -electron delocalization in the molecule (Fig. 19 b).⁹⁷ This was accompanied by a strong red fluorescence emission at ~630 nm at 347 nm excitation, resulting from the structural-conversion to the MC state (Fig. 19 c). These observations were in quite good accordance with those reported in the literature, wherein the water contact angles of photochromic hydrogel

surfaces with MC state isomers decreased relative to those of SP isomers, showing that the surface wettability of the photochromic hydrogel is controllable by light.¹⁰⁹



Picture 3. Visual changes to the sample upon irradiation of 365 nm UV light for 3 min.

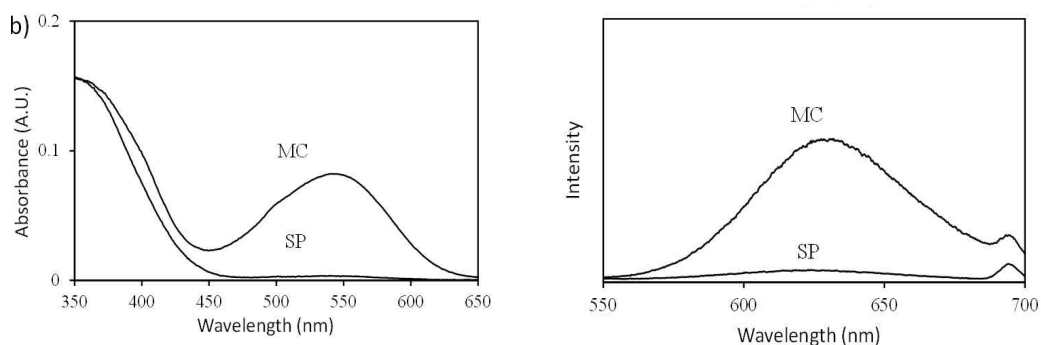


Figure 19. Absorbance spectra of SP-IPN-H before and after UV irradiation (left). Fluorescence spectra illustrating the isomerization of SP and MC (right) ($\lambda_{ex} = 347\text{nm}$).

The reverse photo-responsive isomerization of SP molecules in the hydrogels was investigated under white LED irradiation. After exposure to LED light, the purple hydrogels turned colorless and the distinct absorbance peak at 550 nm disappeared, suggesting that the ring-closed SP form was predominant, thus demonstrating their photochromic reversibility. The resultant colorless hydrogel also showed a decreased emission peak at 630 nm when excited at 347 nm, indicative of the formation of the SP form (Fig. 21c).

Figure 21b shows the UV/Vis spectra of the hydrogels acidified with HCl vapor for 3 min and stored in the dark. The purple hydrogel gradually

faded and turned dime-yellow in color corresponding to the strong absorbance band with peaks at ~400-470 nm. This decolorization was attributed to the protonated form of MC, MCH, which is a stable ring-open isomer formed under acidic conditions.⁹⁴ The hydrogel with the MCH form was non-fluorescent under UV light because the protonation of the phenolate ion in the MC form significantly decreased the efficiency of fluorescence emission.

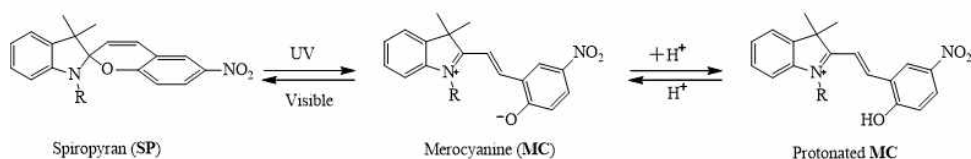
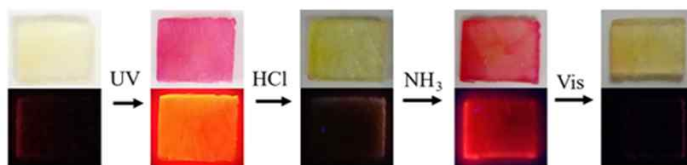


Figure 20. The changes in the spiropyran structure with light irradiation and exposure to acid/base gases.



Picture 4. Visual changes in SP-IPN-H as it responded to light and HCl/NH₃ gases.

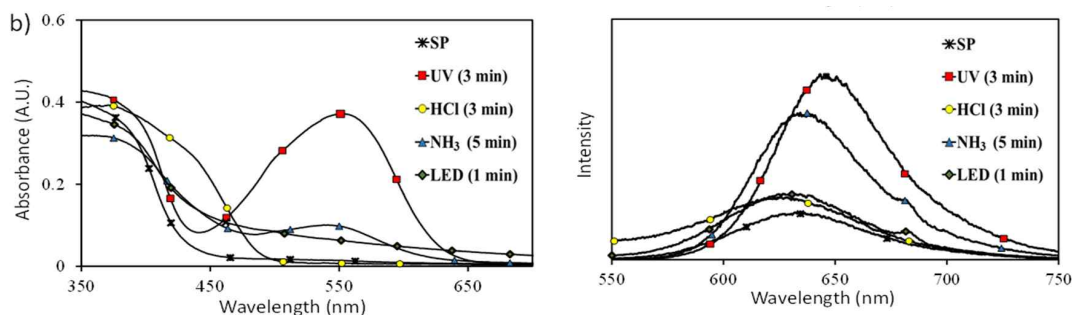


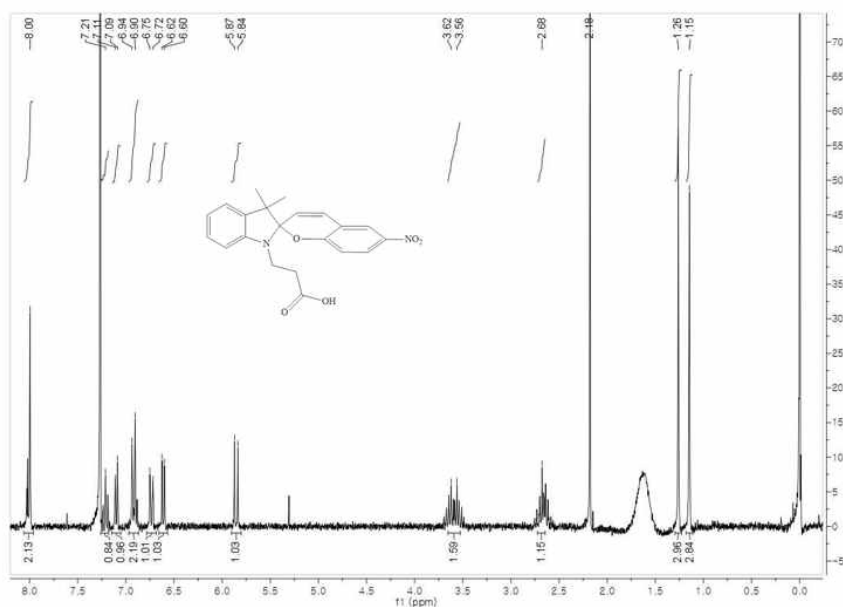
Figure 21. Corresponding absorbance spectra of SP-IPN-H (left). Fluorescence spectra of SP-IPN-H (right) ($\lambda_{\text{ex}} = 347\text{nm}$).

By neutralizing the acidic hydrogels with NH₃ gas, the hydrogel, which had been yellowish under acidic conditions, turned purple within 5 min,

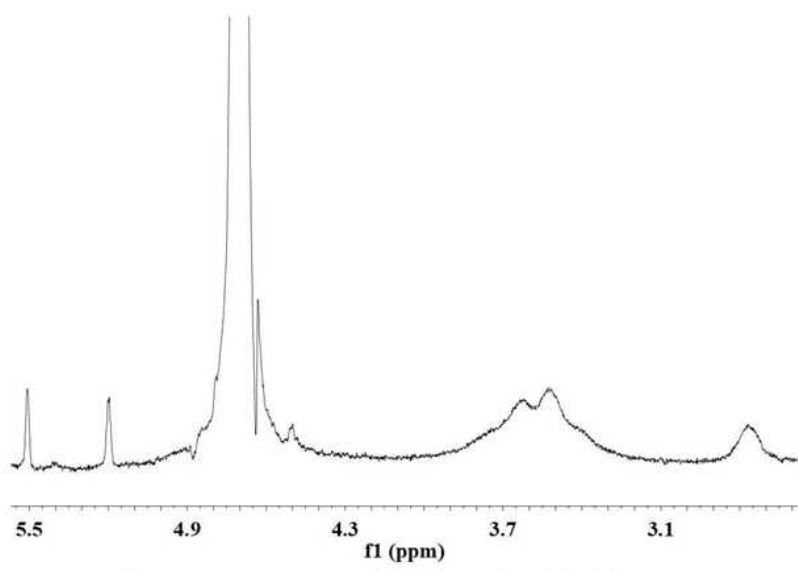
and regained its former color within a moment when acidified by treatment with HCl gas. Usually, photochromic materials that isomerize in response to stimuli, including SP derivatives, need enough space to change their structures.¹¹⁰ Herein, chitosan-IPN structures on p(HEMA) hydrogels proved to be an excellent matrix for the spatial structural changes of the SP molecules. The surface-immobilized SP molecules were able to interchange between their isomers, producing photochromic and fluorescent hydrogels. Furthermore, the protonation and deprotonation processes of the hydrogel that resulted in the color changes could be performed at least five times.

4. Conclusions

In summary, we developed a novel method leading to the formation of multi-responsive hydrogels that changed their color and fluorescence upon UV illumination or acid-base treatment. The p(HEMA)-based hydrogels were synthesized first and then interpenetrated with methacrylamide chitosan polymers. The cross-linking reactions between the chitosan backbones yielded the chitosan-IPN structures consisting of chitosan networks and the p(HEMA) matrix. Further SP-modification resulted in the multi-responsive photochromic hydrogels. With UV irradiation, the colorless SP on the hydrogel isomerized to its purple fluorescent MC form. In addition, the MC form could be protonated by treatment with HCl vapor, resulting in a yellow hydrogel. This acid-derived process, in turn, could be reversed by NH_3 treatment, giving rise to a purple hydrogel. The results described herein provide a useful strategy to develop photochromic optical devices and chemical sensors.



¹H NMR of Spiropyran-propionic acid



¹H NMR of methacrylamide chitosan

References

- [1] Alan R. Hibbs / In *Confocal Microscopy for Biologists* (2004) 259
- [2] David M. Jameson, John C. Croney, and Pierre DJ Moens / In *Methods in enzymology* 360 (2003) 1
- [3] Chenchen Yang, Jun Zhang, Wei-Tao Peng, Wei Sheng, Dianyi Liu, Padmanaban S. Kuttipillai, Margaret Young et al. / *Scientific reports* 1 (2018) 16359
- [4] Matthew Clark, ed. / *Handbook of textile and industrial dyeing: principles, processes and types of dyes* 2011
- [5] Juan F. Araneda, Warren E. Piers, Belinda Heyne, Masood Parvez, and Robert McDonald / *Angewandte Chemie International Edition* 51 (2011) 12214
- [6] Alexander V. Fonin, Anna I. Sulatskaya, Irina M. Kuznetsova, and Konstantin K. Turoverov / *PLoS One* 7 (2014) e103878
- [7] Ana Mendonça, Ana C. Rocha, Armando C. Duarte, and Eduarda BH Santos / *Analytica chimica acta* 788 (2013) 99
- [8] Xavier Luciani, Stéphane Mounier, Roland Redon, and André Bois / *Chemometrics and Intelligent Laboratory Systems* 2 (2009) 227
- [9] Mikhail Y. Berezin, and Samuel Achilefu / *Chemical reviews* 5 (2010) 2641
- [10] Jihad René Albani / *Principles and applications of fluorescence spectroscopy* 8 (2007)
- [11] Christian Würth, Markus Grabolle, Jutta Pauli, Monika Spieles, and Ute Resch-Genger / *Nature protocols* 8 (2013) 1535
- [12] Rongrong Hu, Erik Lager, Angélica Aguilar-Aguilar, Jianzhao Liu, Jacky WY Lam, Herman HY Sung, Ian D. Williams et al. / *The Journal of Physical Chemistry C* 36 (2009) 15845
- [13] Xiaolong Sun, Tony D. James, and Eric V. Anslyn / *Journal of the American Chemical Society* 6 (2018) 2348
- [14] Jye-Shane Yang, and Jyu-Lun Yan / *Chemical Communications* 13 (2008) 1501
- [15] Chung-Wen Wu, Chien-Min Tsai, and Hong-Cheu Lin / *Macromolecules* 13 (2006) 4298
- [16] Guo-Feng Zhang, Ze-Qiang Chen, Matthew P. Aldred, Zhe Hu, Tao Chen, Zhenli Huang, Xianggao Meng, and Ming-Qiang Zhu / *Chemical Communications* 81 (2014) 12058
- [17] Yuning Hong, Jacky WY Lam, and Ben Zhong Tang / *Chemical communications* 29 (2009) 4332

- [18] Nelson LC Leung, Ni Xie, Wangzhang Yuan, Yang Liu, Qunyan Wu, Qian Peng, Qian Miao, Jacky WY Lam, and Ben Zhong Tang / *Chemistry-A European Journal* 47 (2014) 15349
- [19] Aurore Loudet, and Kevin Burgess / *Chemical reviews* 11 (2007) 489
- [20] Claire Tonnelé / "Chemical Sensors: Modelling the Photophysics of Cation Detection by Organic Dyes." PhD diss., Université Sciences et Technologies-Bordeaux I, 2013.
- [21] Noël Boens, Volker Leen, Wim Dehaen, Lina Wang, Koen Robeyns, Wenwu Qin, Xiaoliang Tang et al / *The Journal of Physical Chemistry A* 39 (2012) 9621
- [22] Minkyu Kyeong, Jinho Lee, Kwanghee Lee, and Sukwon Hong / *ACS applied materials & interfaces* 27 (2018) 23254
- [23] Roland Gresser, Horst Hartmann, Marion Wrackmeyer, Karl Leo, and Moritz Riede / *Tetrahedron* 37 (2011) 7148
- [24] Luke D. Lavis, and Ronald T. Raines / *ACS chemical biology* 3 (2008) 142
- [25] Laura M. Wysocki, and Luke D. Lavis / *Current opinion in chemical biology* 6 (2011) 752
- [26] Lingling Li, Junyan Han, Binh Nguyen, and Kevin Burgess / *The Journal of organic chemistry* 5 (2008) 1963
- [27] Shilei Zhu, Jingtuo Zhang, Giri Vegesna, Fen-Tair Luo, Sarah A. Green, and Haiying Liu / *Organic letters* 3 (2010) 438
- [28] Daniel Collado, Yolanda Vida, Francisco Najera, and Ezequiel Perez-Inestrosa / *Rsc Advances* 5 (2014) 2306
- [29] Alexandra M. Courtis, Sofia A. Santos, Yinghua Guan, J. Adam Hendricks, Balaram Ghosh, D. Miklos Szantai-Kis, Surya A. Reis, Jagesh V. Shah, and Ralph Mazitschek / *Bioconjugate chemistry* 6 (2014) 1043
- [30] Xin-Dong Jiang, Jian Zhang, Taniyuki Furuyama, and Weili Zhao / *Organic letters* 1 (2011) 248
- [31] Yu Gabe, Tasuku Ueno, Yasuteru Urano, Hirotatsu Kojima, and Tetsuo Nagano / *Analytical and bioanalytical chemistry* 3 (2006) 621
- [32] Chouaib Tahtaoui, Cécile Thomas, François Rohmer, Philippe Klotz, Guy Duportail, Yves Mély, Dominique Bonnet, and Marcel Hibert / *The Journal of organic chemistry* 1 (2007) 269
- [33] Manal L. Louka, Hebatallah Said, Sara El Sayed, and Mohamed El-Shinawi / *Gene Reports* 7 (2017) 184
- [34] Emilia C. Calvaresi, and Paul J. Hergenrother / *Chemical science* 6 (2013) 2319

- [35] Yuxiang Ma, Haiyan Chen, Shanyuhan Su, Tong Wang, Congying Zhang, Guissi Fida, Sisi Cui, Juan Zhao, and Yueqing Gu / *Journal of Cancer* 7 (2015) 658
- [36] Neelam Shivran, Mrityunjay Tyagi, Soumyaditya Mula, Pooja Gupta, Bhaskar Saha, Birija S. Patro, and Subrata Chattopadhyay / *European journal of medicinal chemistry* 122 (2016) 352
- [37] Li Quan, Shi Liu, Tingting Sun, Xingang Guan, Wenhai Lin, Zhigang Xie, Yubin Huang, Yiqing Wang, and Xiabin Jing / *ACS applied materials & interfaces* 18 (2014) 16166
- [38] Xuehua Hong, Zhuyuan Wang, Jing Yang, Qingdong Zheng, Shenfei Zong, Yu Sheng, Deqin Zhu, Changquan Tang, and Yiping Cui / *Analyst* 18 (2012) 4140
- [39] Zhuyuan Wang, Xuehua Hong, Shenfei Zong, Changquan Tang, Yiping Cui, and Qingdong Zheng / *Scientific reports* 5 (2015) 12602
- [40] Si Zhang, Tong Wu, Jiangli Fan, Zhiyong Li, Na Jiang, Jingyun Wang, Bairui Dou, Shiguo Sun, Fengling Song, and Xiaojun Peng / *Organic & biomolecular chemistry* 4 (2013) 555
- [41] Bosung Kim, Binglin Sui, Xiling Yue, Simon Tang, Michael G. Tichy, and Kevin D. Belfield / *European Journal of Organic Chemistry* 1 (2017) 25
- [42] Tao Gao, Huan He, Rong Huang, Mai Zheng, Fang-Fang Wang, Yan-Jun Hu, Feng-Lei Jiang, and Yi Liu / *Dyes and Pigments* 141 (2017) 530
- [43] Chin Siang Kue, Shie Yin Ng, Siew Hui Voon, Anyanee Kamkaew, Lip Yong Chung, Lik Voon Kiew, and Hong Boon Lee / *Photochemical & Photobiological Sciences* 11 (2018) 1691
- [44] Zhuo Ye, Chao Xiong, Jian Pan, Dongdong Su, and Lintao Zeng / *Dyes and Pigments* 155 (2018) 30
- [45] Dnyaneshwar Kand, Tanmoy Saha, Mayurika Lahiri, and Pinaki Talukdar / *Organic & biomolecular chemistry* 30 (2015) 8163
- [46] Mengliang Zhu, Peipei Xing, Yabin Zhou, Lei Gong, Jinghui Zhang, Dongdong Qi, Yongzhong Bian, Hongwu Du, and Jianzhuang Jiang / *Journal of Materials Chemistry B* 27 (2018) 4422
- [47] Lech-Gustav Milroy, Stefano Rizzo, Abram Calderon, Bernhard Ellinger, Silke Erdmann, Justine Mondry, Peter Verveer et al. / *Journal of the American Chemical Society* 20 (2012) 8480
- [48] Philip A. Waghorn, Michael W. Jones, Alan McIntyre, Alessio Innocenti, Daniela Vullo, Adrian L. Harris, Claudiu T. Supuran, and Jonathan R. Dilworth / *European Journal of Inorganic Chemistry* 17 (2012) 2898
- [49] Michael L. Vetter, Zijuan Zhang, Shuai Liu, Jinhua Wang, HaeYeon Cho, Jianming Zhang, Wei Zhang, Nathanael S. Gray, and Priscilla L. Yang / *ChemBioChem* 9 (2014) 1317

- [50] Sanjeev Kumar, V. Vernekar, Hasan Y. Hallaq, Guy Clarkson, Andrew J. Thompson, Linda Silvestri, Sarah CR Lummis, and Martin Lochner / *Journal of medicinal chemistry* 5 (2010) 2324
- [51] Taisuke Katoh, Masato Yoshikawa, Takeshi Yamamoto, Ryosuke Arai, Noriyuki Nii, Yoshihide Tomata, Shinkichi Suzuki, Ryoukichi Koyama, Nobuyuki Negoro, and Takatoshi Yogo / *Bioorganic & medicinal chemistry letters* 5 (2017) 1145
- [52] Guanglei Li, Yu Otsuka, Takuya Matsumiya, Toshiyuki Suzuki, Jianye Li, Masashi Takahashi, and Koji Yamada / *Materials* 8 (2018) 1297
- [53] R. D. Moriarty, A. Martin, K. Adamson, E. O'reilly, P. Mollard, R. J. Forster, and T. E. Keyes / *Journal of microscopy* 3 (2014) 204
- [54] Onur Buyukcakir, O. Altan Bozdemir, Safacan Kolemen, Sundus Erbas, and Engin U. Akkaya / *Organic letters* 20 (2009) 4644
- [55] Luke D. Lavis, and Ronald T. Raines / *ACS chemical biology* 4 (2014) 855–866
- [56] Tian-Bing Ren, Wang Xu, Wei Zhang, Xing-Xing Zhang, Zhi-Yao Wang, Zhen Xiang, Lin Yuan, and Xiao-Bing Zhang / *Journal of the American Chemical Society* 24 (2018) 7716
- [57] Xiaojun Peng, Fengling Song, Erhu Lu, Yanan Wang, Wei Zhou, Jiangli Fan, and Yunling Gao / *Journal of the American Chemical Society* 12 (2005) 4170
- [58] Meijuan Jiang, Xingguo Gu, Jacky WY Lam, Yilin Zhang, Ryan TK Kwok, Kam Sing Wong, and Ben Zhong Tang / *Chemical science* 8 (2017) 5440
- [59] Vikas S. Padalkar, and Shu Seki / *Chemical Society Reviews* 1 (2016) 169
- [60] Xingyu Qu, Quan Liu, Xiaoning Ji, Huachao Chen, Zhikuan Zhou, and Zhen Shen / *Chemical Communications* 38 (2012) 4600
- [61] Amy M. Bittel, Ashley M. Davis, Lei Wang, Michel A. Nederlof, Jorge O. Escobedo, Robert M. Strongin, and Summer L. Gibbs / *Scientific reports* 1 (2018) 4590
- [62] Cornelis J. Weijer / *Science* 5616 (2003) 96
- [63] Ben NG Giepmans, Stephen R. Adams, Mark H. Ellisman, and Roger Y. Tsien / *Science* 5771 (2006) 217
- [64] Mikael J. Pittet and Ralph Weissleder / *Cell* 5 (2011) 983
- [65] Ronald N. Germain, Ellen A. Robey, and Michael D. Cahalan / *Science* 6089 (2012) 1676
- [66] Seung Hwan Lee, Hoa Thi Bui, Temmy Pegarro Vales, Sung Cho, and Ho-Joong Kim / *Dyes and Pigments* 145 (2017) 216
- [67] Duy Khuong Mai, Joomin Lee, Ilgi Min, Temmy Vales, Kyong-Hoon Choi, Bong Park, Sung Cho, and Ho-Joong Kim / *Nanomaterials* 9 (2018) 728

- [68] Toshiyuki Kowada, Hiroki Maeda, and Kazuya Kikuchi / *Chemical Society Reviews* 14 (2015) 4953
- [69] Hongde Xiao, Jianhui Li, Kaitian Wu, Gui Yin, Yiwu Quan, and Ruiyong Wang / *Sensors and Actuators B: Chemical* 213 (2015) 343
- [70] Alexander B. Nepomnyashchii, Allen J. Pistner, Allen J. Bard, and Joel Rosenthal / *The Journal of Physical Chemistry C* 11 (2013) 5599
- [71] Lijuan Jiao, Changjiang Yu, Timsy Uppal, Mingming Liu, Yan Li, Yunyou Zhou, Erhong Hao, Xiaoke Hu, and M. Graça H. Vicente / *Organic & biomolecular chemistry* 11 (2010) 2517
- [72] Xin-Dong Jiang, Ruina Gao, Yi Yue, Guo-Tao Sun, and Weili Zhao / *Organic & biomolecular chemistry* 34 (2012) 6861
- [73] Timsy Uppal, Xiaoke Hu, Frank R. Fronczek, Stephanie Maschek, Petia Bobadova-Parvanova, and M. Graça H. Vicente / *Chemistry-A European Journal* 13 (2012) 3893
- [74] Yen Vo-Hoang, Laurent Micouin, Catherine Ronet, Gabriel Gachelin, and Martine Bonin / *ChemBioChem* 1 (2003) 27
- [75] Sheel C. Dodani, Qiwen He, and Christopher J. Chang / *Journal of the American Chemical Society* 50 (2009) 18020
- [76] Song Lin Niu, Gilles Ulrich, Raymond Ziessel, Agneta Kiss, Pierre-Yves Renard, and Anthony Romieu / *Organic letters* 10 (2009) 2049
- [77] Lijuan Jiao, Jilong Li, Shengzhou Zhang, Chao Wei, Erhong Hao, and M. Graça H. Vicente / *New Journal of Chemistry* 9 (2009) 1888
- [78] Anthony Romieu, Cédrik Massif, Sandra Rihn, Gilles Ulrich, Raymond Ziessel, and Pierre-Yves Renard / *New Journal of Chemistry* 4 (2013) 1016
- [79] M. Gonçalves and Sameiro T / *Chemical reviews* 1 (2008) 190
- [80] Xiaodong Liu, Bizheng Chen, Xiaojun Li, Lifeng Zhang, Yujie Xu, Zhuang Liu, Zhenping Cheng, and Xiulin Zhu / *Nanoscale* 39 (2015) 16399
- [81] Yuichi Kajiwara, Atsushi Nagai, and Yoshiki Chujo / *Journal of Materials Chemistry* 15 (2010) 2985
- [82] R., N Nguyen, Jouault, S. Zanirati, M. Rawiso, L. Allouche, G. Fuks, E. Buhler, and N. Giuseppone / *Soft matter* 22 (2014) 3926
- [83] Protocol. *Promega, USA* (2001).
- [84] Sascha Hoogendoorn, Annet EM Blom, Lianne I. Willems, Gijbert A. van der Marel, and Herman S. Overkleeft / *Organic letters* 20 (2011) 5656
- [85] Yuezhi Mao, Martin Head-Gordon, and Yihan Shao / *Chemical science* 45 (2018) 8598

- [86] I. K. Petrushenko, and K. B. Petrushenko / *Spectrochimica Acta Part A: Molecular and Biomolecular Spectroscopy* 138 (2015) 623
- [87] Ying Li, Hechun Lin, Chunhua Luo, Yunqiu Wang, Chunli Jiang, Ruijuan Qi, Rong Huang, Jadranka Travas-sejdic, and Hui Peng / *Rsc Advances* 51 (2017) 32225
- [88] Ana Katrina Estandarte, Stanley Botchway, Christophe Lynch, Mohammed Yusuf, and Ian Robinson / *Scientific reports* 6 (2016) 31417
- [89] Dong-Hoon Choi, Si-Young Ban, and Jae-Hong Kim / *Bulletin of the Korean Chemical Society* 4 (2003) 441
- [90] Lukas Baumann, Katrin Schöller, Damien de Courten, Dominik Marti, Martin Frenz, Martin Wolf, René M. Rossi, and Lukas J. Scherer / *RSC advances* 45 (2013) 23317
- [91] Young Min Kho, Dae Young Hur, and Eun Ju Shin / *Bulletin of the Korean Chemical Society* 10 (2016) 1728
- [92] Yu Huang, Fengyu Li, Changqing Ye, Meng Qin, Wei Ran, and Yanlin Song / *Scientific reports* 5 (2015) 9724
- [93] Lei Chen, Yu Zhu, Danling Yang, Rongfeng Zou, Junchen Wu, and He Tian / *Scientific reports* 4 (2014) 6860
- [94] Yoon-Seung Nam, Imsung Yoo, Oktay Yarimaga, In Sung Park, Dong-Hoon Park, Simon Song, Jong-Man Kim, and Chan Woo Lee / *Chemical Communications* 32 (2014) 4251
- [95] Chang Hoon Jeon, and Tai Hwan Ha / *Bulletin of the Korean Chemical Society* 3 (2015) 1054
- [96] Hyeri Chang, Jong Pil Lee, and Jong-Man Kim / *Bulletin of the Korean Chemical Society* 12 (2016) 2047
- [97] Rafal Klajn / *Chemical Society Reviews* 1 (2014) 148
- [98] Shulin Wan, Yang Zheng, Jie Shen, Wantai Yang, and Meizhen Yin / *ACS applied materials & interfaces* 22 (2014) 19515
- [99] Larisa Florea, Dermot Diamond, and Fernando Benito-Lopez / *Macromolecular Materials and Engineering* 12 (2012) 1148
- [100] Dae Young Hur, and Eun Ju Shin / *Bulletin of the Korean Chemical Society* 10 (2013) 3125
- [101] Keun-Seung Jeong, Ho-Joong Kim, Hwa-Lim Lim, Geun-Chang Ryu, Eun-Sun Seo, Nam-Ho You, and Jin Jun / *Bulletin of the Korean Chemical Society* 6 (2015) 1649
- [102] Itsuro Tomatsu, Ke Peng, and Alexander Kros / *Advanced drug delivery reviews* 14-15 (2011) 1257

- [103] Pietro Matricardi, Chiara Di Meo, Tommasina Coviello, Wim E. Hennink, and Franco Alhaique / *Advanced Drug Delivery Reviews* 9 (2013) 1172
- [104] Preeti K. Suresh, Satish K. Suryawani, and Divya Dewangan / *Pharmacie Globale Int. J. Compr. Pharm* 8 (2011) 1
- [105] Sema Ekici, and Dursun Saraydin / *Polymer International* 11 (2007) 1371
- [106] K. Kumari, and P. P. Kundu / *Bulletin of Materials Science* 2 (2008) 159
- [107] Laura MY Yu, Karineh Kazazian, and Molly S. Shoichet / *Journal of Biomedical Materials Research Part A* 1 (2007) 243
- [108] Cheol Woo Lee, Seung Hwan Lee, Young-Keun Yang, Geun-Chang Ryu, and Ho-Joong Kim / *Journal of Applied Polymer Science* 30 (2017) 45120.
- [109] Lie Chen, Xi Yao, Zhandong Gu, Kaikai Zheng, Chuangqi Zhao, Wenwei Lei, Qinfeng Rong et al. / *Chemical science* 3 (2017) 2010
- [110] Pintu K. Kundu, Gregory L. Olsen, Vladimir Kiss, and Rafal Klajn / *Nature communications* 5 (2014) 3588.

Acknowledgements

I would like to extend my gratitude to all the people who were directly and indirectly involved in the completion of this work. I am grateful to my supervisor, Prof. Kim Ho-Joong, for his patience, knowledge and invaluable input for this work. I also thank my colleagues, Temmy Vales and Mai Khoung Duy for their help and companionship. Lastly, I thank my family and friends for their unfailing support of my endeavors.